Thesis for the Degree of Doctor of Philosophy

Observed and Simulated Changes in Extreme Precipitation and Cold Surges in China: 1961-2005

Tinghai Ou

UNIVERSITY OF GOTHENBURG

Faculty of Science

Doctor Thesis A146
University of Gothenburg
Department of Earth Sciences
Gothenburg, Sweden 2013

Tinghai Ou

Observed and Simulated Changes in Extreme Precipitation and Cold Surges in China: 1961-2005

A146 2013
ISBN: 978-91-628-8627-1
ISSN: 1400-3813
Internet-id: http://hdl.handle.net/2077/31816
Printed by Kompendiet

Distribution: Department of Earth Sciences, University of Gothenburg, Sweden

ABSTRACT

In the present work, precipitation and temperature related climate extremes are examined, with a focus on Mainland China. The objectives of this study are a) to identify targeted climate extremes and their changes during the last decades, and b) to examine the ability of current global climate models to reproduce identified patterns of change.

The observed change in extreme precipitation from 1961 to 2000 is investigated using a set of indices, and the change simulated by global climate models is evaluated. In order to find an appropriate gridding method for the extreme indices in model evaluations, the effects of two different methods for estimating indices from station data are examined: one set interpolated from indices at stations (EI_{STA}) and the other calculated from gridded precipitation (EI_{GRID}). Results show that there is a large difference between the two, especially at coarser resolution, and suggests that EI_{GRID} indices are more appropriate to evaluate model simulated precipitation extremes. During the period in question, observed extreme precipitation amounts increased in most parts of China, the only exception being northern China, where there was a decreasing trend. The trend of consecutive dry days (CDD) observed there is generally opposite to that of extreme precipitation elsewhere in China, except in southeast China, where both extreme precipitation and CDD increased. Most of the studied global climate models tend to overestimate extreme precipitation amounts but underestimate CDD. The pattern of precipitation extremes is generally well captured in western China, while in eastern China, where the combination of the monsoon system and human activities (e.g., anthropogenic changes in land use and aerosols) affects climate variation, with the result that climate patterns are reproduced poorly by comparison.

In regard to temperature-related extremes, the variation in the occurrence of winter cold surges in southeast China for the period from 1961 to 2005 is investigated. The identified cold surges are divided into 5 different groups based on the evolution pattern of the Siberian High (SH). Associated evolutions of the large-scale atmospheric circulation are investigated. Results suggest the importance of a SH amplification and pre-existing specific synoptic systems to the occurrence of cold surges. Investigating the long-term changes in cold surges of different groups, it is found that the SH-related cold surges (33%) have decreased in the last 20 years, while cold surges more closely associated with background atmospheric circulation systems, which often have a larger impact area (i.e., stronger cold air outbreak) than the SH-related ones, have increased since the early 1980s. Although the intensity of SH was relatively weak with warmer surface air temperatures over China during the period from 1980 to 2005, the total number of cold surges in this period was nearly identical to that of previous decades. This implies that future occurrences of cold surges in southeast China may remain at current levels, provided that the contribution from the SH-related surges does not change dramatically.

Keywords: Climate extremes, Precipitation, Cold surge, Siberian High, CMIP5, reanalysis, atmospheric circulation

PREFACE

This thesis consists of a summary (Part I) followed by four appended papers (Part II), referred to by roman numerals in the text:

I. Paper I

Chen, D., **T. Ou**, L. Gong, C.-Y. Xu, W. Li, C.-H. Ho, and W. Qian (2010), Spatial interpolation of daily precipitation in China: 1951-2005. ***Advances in atmospheric Sciences***, 27, 1221-1232.

T. Ou collected the data, conducted the analysis, visualized the results, and contributed to the writing.

II. Paper II

Ou, T., D. Chen, H. W. Linderholm, and J.-H. Jeong (2012), Evaluation of climate models in simulating extreme precipitation in China. (Submitted to ***Tellus A***)

T. Ou initiated the paper, conducted the analysis, visualized the results, and contributed the bulk of the writing.

III. Paper III

Jeong, J.-H., **T. Ou**, H. W. Linderholm, B.-M. Kim, S.-J. Kim, J.-S. Kug, and D. Chen (2011), Recent recovery of the Siberian High intensity. ***J. Geophys. Res.***, 116, D23102, doi:10.1029/2011JD015904.

T. Ou collected the data, conducted the analysis, visualized the results, and contributed to the writing.

IV. Paper IV

Ou, T., D. Chen, J.-H. Jeong, and H. W. Linderholm (2012), Variation of winter cold surges in southeast China and their relationship with atmospheric circulation patterns. (*Manuscript*)

T. Ou initiated the paper, conducted the analysis, visualized the results, and contributed the bulk of the writing.

Scientific publications which are not included in this thesis:

Linderholm, H. W., A. Seim, **T. Ou**, J.-H. Jeong, L. Yu, X. Wang, G. Bao, and C. Folland (2012), Exploring teleconnections between the summer NAO (SNAO) and climate in East Asia over the last four centuries - a tree-ring perspective. ***Dendrochronologia***. (accepted)

Ou, **T.**, Y. Liu, D. Chen, D. Rayner, Q. Zhang, G. Gao, and W. Xiang (2011), The influence of large-scale circulation on the summer hydrological cycle in the Haihe River basin of China. ***Acta Meteor. Sinica***, 25, 517-526, doi: 10.1007/s13351-011-0410-3.

Duan, X., Y. Xie, **T. Ou**, and H. Lu (2011), Effects of soil erosion on long-term soil productivity in the black soil region of northeastern China. ***CATENA***, 87, 268-275, doi:10.1016/j.catena.2011.06.012.

Linderholm, H. W., **T. Ou**, J.-H. Jeong, C. K. Folland, D. Gong, H. Liu, Y. Liu, and D. Chen (2011), Interannual teleconnections between the summer North Atlantic Oscillation and the East Asian summer monsoon. ***J. Geophys. Res.***, 116, D13107, doi:10.1029/2010JD015235.

Tang, L., D. Chen, P.E. Karlsson, Y. Gu, and **T. Ou** (2009), Synoptic circulation and its influence on spring and summer surface ozone concentrations in southern Sweden. ***Boreal Env. Res.,*** 14, 889-902.

Chen, D., C. Achberger, U. Postgård, A. Walther, Y. Liao, and **T. Ou** (2008), Using a weather generator to create future daily precipitation scenarios for Sweden. ***Research Report*** C76, Earth Sciences Centre, University of Gothenburg, Gothenburg, Sweden, 82 pp.

Contents

I. Summary

II. Papers I-IV

Part I

Summary

1. Introduction

1.1. Climate extremes and their significance

An extreme weather event, according to the IPCC (2007), is "an event that is rare at a particular place and time of year. Definitions of rare vary, but an extreme weather event would normally be as rare as or rarer than the 10th or 90th percentile of the observed probability density function. By definition, the characteristics of what is called extreme weather may vary from place to place in an absolute sense. When a pattern of extreme weather persists for some time, such as a season, it may be classed as an extreme climate event, especially if it yields an average or total that is itself extreme (e.g., drought or heavy rainfall over a season)". As noted in the definition, the distinction between an extreme weather event and an extreme climate event is not precise, but is related to their specific time scales: an extreme weather event typically occurs within a time-scale of approximately one week, and an extreme climate event typically occurs within a time scale longer than a week and up to as long as a season. For simplicity, both extreme weather events and extreme climate events can be referred to by term "climate extremes", such as in IPCC (2012).

Climate extremes often cause great economic damage to infrastructure and property (Munich-Reinsurance 2002), and consequently both the detection and the prediction of extreme climate events are important topics in climate research (Easterling et al. 2000; Kunkel et al. 1999; Meehl et al. 2000). In particular, precipitation and temperature-related climate extremes have been widely examined to understand their past, present and future variability. During the past 50 years, global observations generally show an increasing trend in warmer days and a decreasing trend in colder days over most land areas. Also there is an increasing trend in extreme heavy precipitation events over many areas of the globe, even though the total precipitation is decreasing in many parts of the world (Easterling et al. 2000; Hegerl et al. 2006; Rummukainen 2012). It is expected that these trends will very likely continue into the 21st century (IPCC 2012). The global change in temperature-related extremes and, though less conclusively, the intensification of extreme precipitation on the global scale are regarded to be influenced by anthropogenic climate forcings (IPCC 2012).

1.2 Extreme precipitation

Extreme precipitation is one of the most important variables for practical needs, but it is very difficult to define due to its weak spatial coherence (Alexander et al. 2006; Frich et al. 2002). Extreme precipitation events are often described by defining indices based on precipitation rate (Chen et al. 2006; Moberg et al. 2006), such as consecutive dry days (CDD) and amount of extreme heavy precipitation (top 5 percentile (R95pTOT) and top 1 percentile (R99pTOT) in the total record), etc. For numerous scientific and practical purposes (e.g., examining regional trends and evaluating model simulations), extreme precipitation indices on regular spacing grids are often needed (Alexander et al. 2006; Kiktev et al. 2003). Thus, extreme precipitation estimated from station-based observations has to be converted into gridded values. Generally, there are two ways to obtain gridded extreme precipitation indices (Chen and Knutson 2008): a) first calculating indices from daily observations for all available stations, and then interpolating the indices into different horizontal resolutions (here referred to as EI_{STA}, this method will be further explained in section 3.1.1), and b) first interpolating daily station observations into different horizontal resolutions (area-mean precipitation) and then calculating extreme precipitation indices based on the gridded precipitation (EI_{GRID} hereafter, see section 3.1.1). Results have shown that the difference between the two approaches can be significant (Chen and Knutson 2008).

Despite large uncertainties in the model projections, global climate model simulations are virtually the only means to project future changes in extreme precipitation. There are three main sources of uncertainty: the natural variability of climate; uncertainties in climate model parameters and structure; and projections of future emissions. For precipitation-related extremes, the uncertainties in projected changes by the end of the 21st century are due mainly to uncertainties in the climate models rather than in future emissions scenarios (IPCC 2012). The uncertainty in the projections of extreme precipitation is even larger on regional scale. On the other hand, the horizontal resolution of models may also influence the utility of models in simulation precipitation extremes (Chen and Knutson 2008; Walther et al. 2013). Therefore, the ability of global climate models to simulate extreme precipitation is investigated very carefully when we interpret the regional scale projection of the models.

1.2.1 Extreme precipitation in China

China is frequently hit by extreme precipitation events (e.g. floods and droughts), which cause significant economic and societal disruptions (Zhai et al. 2008). As an example, the floods in 1998 caused $36 billion in economic losses and killed more than 3000 people in the Yangtze River valley in southern China and in the Nenjiang-Songhuajiang valley in Northeast China (NCC, 1998). The frequency of such events is predicted to increase in association with climate warming (Feng et al. 2011; Gong and Wang 2000; Qian et al. 2007a).

Observations of the past 50 years have shown that both extreme heavy precipitation days and drought area have increased (Ren et al. 2011). During this same period, days of light rain decreased (Wang et al. 2012), and the ratio of extreme precipitation to mean precipitation has increased (Wang et al. 2012) over most areas of China.

In particular, there is notable difference in regional trends of extreme precipitation over different regions of China (Easterling et al. 2000). The number of rain days has significantly decreased in Eastern China, and increased in northwest China (Wang et al. 2012). The decrease in number of rain days in northern China, which is associated with the decrease in the number of light rain days (Liu et al. 2011), has led to the decrease of total precipitation in this region (Zhai et al. 2008). The decreasing trend in the number of light rain days in east China might be connected to significant regional warming (Qian et al. 2007b), as well as to increases in aerosol concentrations (Qian et al. 2009). Reduced wind speed due to weakened topographic lifting may also have caused decreases in light rainfall over mountain areas (Yang and Gong 2010).

The frequency of extreme heavy precipitation days increased in southern and northwest China and decreased in northern China (You et al. 2011; Zhai et al. 2005). This is similar to the pattern of the total precipitation. The increase of precipitation intensity and extreme precipitation have led to an increase in total precipitation in the mid-lower reaches of the Yangtze River (Su et al. 2005) and the southeast coast of China (Zhai et al. 2005). There is also an obvious connection to season in the occurrence of extreme heavy precipitation, as there is an increasing trend mainly in winter and a decreasing trend in autumn over the most of China (Wang and Yan 2009; Zhai et al. 2005). Nevertheless, the systematic detection and assessment of changes in extreme heavy precipitation in China remain deficient.

The global climate models from the third phase of the Coupled Model Intercomparison Project (CMIP3) (Meehl et al. 2007) tend to underestimate extreme precipitation in China (Jiang et al. 2011), especially during summer in eastern China where there the extreme precipitation is underestimated by around 50% (Li et al. 2011), and this has important implications for regions such as northern China, where most of the extreme precipitation occurs during the summer wet period (Bai et al. 2007). Due to the fact that climate models are the only means available for projecting the future, there is urgent need to investigate the ability of the new, phase five, CMIP models (CMIP5) (Taylor et al. 2012) to reproduce extreme precipitation in China.

1.3 Cold surges

On global scale, cold surges, which are bringing low temperature extremes, are frequently observed to the east of major north–south oriented mountain ranges, and there are three major cold surge regions, namely Southeast Asia (bordered by the Himalayan Plateau), North and Central America (east of the Rockies and Mexican Sierras), and South America (to the east of the Andes cordillera) (Garreaud 2001, and references therein). The passage of a cold surge is typically characterized by a rapid decrease in air temperatures at low levels accompanied by sharp increases in surface pressure and equatorward low-level winds (Garreaud 2001). In this work, we focus on East Asian cold surges, specifically over southeast China, where there is large population.

Over East Asia, the cold surge is one of the primary subsystems of the East Asian winter monsoon (EAWM) (Jeong et al. 2005). Typically, East Asian cold surges are associated with an abrupt temperature drop and a change of wind direction from easterly to northerly in association with the passage of a cold front. The cold surge in south China is also called the northerly winter monsoon surge (Wu and Chan 1995, 1997). Due to sudden changes in temperature and pressure (Chang et al. 1979; Wu and Chan 1995), occurrences of cold surges can have massive impacts both on the environment and on human activities (Lin et al. 2009; Yang et al. 2009). Cold surges in southeast China often induce intense rainfall (Chen and Ding 2007) and snowfall. As an example, the cold surge that occurred from 10 January to 5 February, 2008, induced extremely damaging frosts, snow, and ice storms in southeast China (Lu et al. 2010; Yang et al. 2010) and caused $24 billion in economic losses, 11867 kilohektare crops damaged, killed 129 people and 4 people lost (DCAS/NCC/CMA 2008; Zhao et al 2008).

In terms of large-scale atmospheric circulation, the onsets of cold surges in East Asia are mostly associated with an intensification and southeast propagation of the Siberian High (SH) (Ding 1990; Wu and Chan 1997) and therefore occurrences of winter cold surges are significantly correlated with the SH intensity (SHI) (Wang and Ding 2006). The SHI is a primary factor in determining the strength of the EAWM circulation; for instance the pressure difference between the SH and the Aleutian low in the North Pacific is used to characterize EAWM circulation (Chang et al. 2006; Wang and Chen 2010). Since early 1970s, significant weakening of both the SH and the EAWM have been followed by obvious increases of winter time temperature and prominent decreases in the frequency of cold surges in East Asia (e.g. Gong and Ho 2002; Panagiotopoulos et al. 2005; Wang and Chen 2010; Wang et al. 2009; Wang and Ding 2006; Zhu 2008). However, there are many other factors which affect the occurrence of cold surges: e.g., the El Nino/Southern Oscillation (ENSO) (Chen et al. 2004; Zhang et al. 1997), the Arctic Oscillation (AO) / North Atlantic Oscillation (NAO) (Hong et al. 2008; Jeong and Ho 2005; Park et al. 2011a), the Madden Julian Oscillation (MJO) (Jeong et al. 2005), and the East Asian jet stream (Chang and Lau 1980; Wu and Chan 1995).

Southeast China is one of the major regions under the significant influence of cold surge occurrences over Mainland China (Ding et al. 2009) and there is relatively high intra-seasonal variability of wintertime temperature (Gong and Ho 2004). In this region, the winter (December-January-February, DJF) mean temperature is generally higher than 5^{o}C (Figure 1.1), which is much higher than temperatures in central and northern Siberia (where winter temperature is usually below -20^{o}C). When there is an eastward and southward propagation of the SH (Zhang and Chen, 1999), the cold air in northern Eurasia is brought into southeast China (i.e., cold surge occurrence) causing a sudden temperature drop in this region (Ding and Krishnamurti 1987; Ding 1990; Zhang and Chen 1999). A recent work by Chen et al. (2004) indicates that there is no clear decreasing trend in the frequency of cold surges over East Asia during the period from 1980 to 2000 and there is even a slight increase in the frequency during the period from 1980 to 2006 (Park et al. 2011b). Some cold surge outbreaks in East Asia may not affect southeast China. Especially during the negative phase of AO, cold surges tend more frequently to occur over Korea and Japan and less frequently over China (Park et al. 2011a). Therefore the change in the occurrence of cold surges in East Asia may not reflect the change in the occurrence of cold in southeast China.

So far, very few studies have focused on the occurrences of winter cold surges in southeast China. The investigation of the variation in the occurrences of cold surges during the past 40 to 50 years, especially during the period since 1980 which has seen the mean temperature in China increase significantly (Liu et al. 2004), remains deficient. Moreover, since the cold surge frequency in East Asia is shown to have been kept stable for the last few decades despite an overall decreasing trend in cold days (Park et al. 2011b), it is of interest to investigate the mechanisms behind this in order to better forecast future changes. Such an investigation requires close understanding of the dynamic mechanisms of cold surges and associated atmospheric circulation patterns.

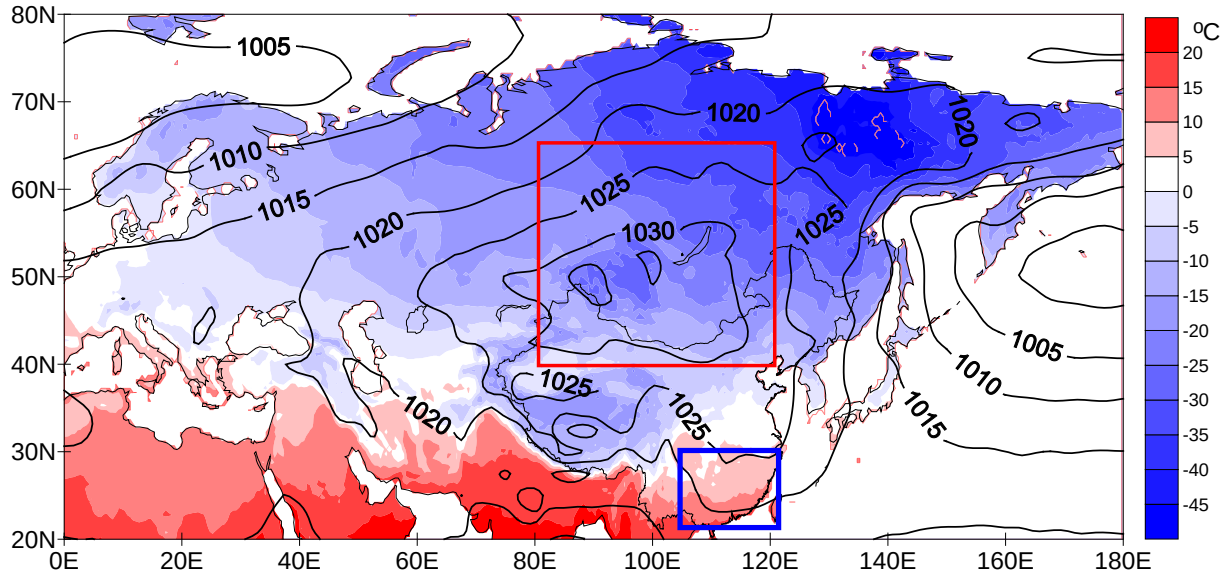

Figure 1.1 Map shows the winter (DJF) mean sea level pressure (SLP: contour) and winter mean 2m temperature (1961-1990 climate mean from CRU (New et al. 1999), shaded) (red square indicates the region used to get the Siberian High intensity (SHI: 40-65N, 80-120E), and the blue square indicates the study region for winter cold surges: south of 30°N and east of 105°E with a focus on southeast China)

1.4 Aims and objectives

The overall aims of this thesis are 1) to improve our understanding of extreme precipitation events in China through observations and climate model simulations of different spatial scales, and 2) to assess recent changes in cold surge events over southeast China associated with large-scale atmospheric circulation changes.

The specific objectives of this work are to

- Examine the effects of two different methods for estimating extreme precipitation indices from station data in order to find the appropriate gridding method for analysing station observations in China,
- Evaluate model-simulated extreme precipitation based on extreme indices with the appropriate gridding method,
- Identify the change in the occurrence of winter cold surges in southeast China during 1961-2005, especially after 1980,
- Improve our understanding of the influence of the atmospheric circulation in the change in cold surge occurrences in southeast China.

The works related to the first two objectives are paper I and paper II. In paper I, several methods for the interpolation of daily precipitation are compared and discussed, and ordinary kriging using seasonal semi-variograms is used to generate a daily gridded precipitation dataset for China from 1951 to 2005. In paper II, the effects of two different methods, EI_{STA} and $EI_{GRID,}$ for estimating extreme precipitation indices from station data is investigated. The EI_{GRID} extreme precipitation indices are used to examine the observed change in extreme precipitations from 1961 to 2000 and to evaluate precipitation simulated by models during the same period. Paper I provides the fundamental methodology, such as the data collection and interpolation etc., utilized in paper II. In this thesis more emphasis will be put on the results from paper II than from paper I.

In papers III and IV, the objectives related to cold surges in southeast China are addressed. In paper III, the change in atmospheric circulation over Eurasia during the past 100 years, with a focus on the most recent 40 year period, is examined and possible explanations discussed. In paper IV, the change in the occurrence of winter cold surges in southeast China from 1961 to 2005 is investigated. Daily and seasonal (winter) atmospheric circulation patterns related to cold surge occurrences are identified, and the influence of atmospheric circulation on cold surge occurrences is addressed. Paper III lays the groundwork for paper IV, and greater attention will be the results of paper IV in this thesis.

2. Data collection and its processing

2.1 Processing of daily station records in China

In this thesis, precipitation and temperature, the two most important meteorological variables, were used to explore observed changes in climate extremes. Detailed information is given in the following parts on the data used.

2.1.1 Daily precipitation

There are 753 national meteorological stations in Mainland China, with observations from 1 January, 1951, to 31 December, 2005 available from the National Meteorological Information Center of the China Meteorological Administration (NMIC/CMA). The station locations range from 16°32'N to 52°58'N, and from 75°14'E to 132°58'E (Figure 2.1), and the altitude of the stations varies from 1.1 m to 4800 m (above sea level). The average distance between stations is 72 km, while between any two the maximal distance is 366 km and the minimum distance is 4 km. The stations cover most of China. However, the station network is denser and more evenly distributed in the southeast (Figure 2.1a). The instrumentally-observed variables related to this work include daily precipitation amounts, daily mean temperatures, and daily minimum temperatures. In this part we focus on the observed daily precipitation amounts.

Before working on the instrumental data, a quality control for the data set is very important. The daily precipitation observations from 1951 to 2000 have previously been checked by Feng et al. (2004) for data homogeneity and consistency. In this study, the daily precipitation data from 1951 to 2005 were screened for outliers, and a few suspicious data were flagged and subsequently treated as missing data. This was done for all stations. Some basic statistical information of the scrutinized data set is given below.

The average percentage of missing data from 1951 to 2005 for the 753 stations is 16.1%. However, stations established before the early 1960s are responsible for the majority of the missing data, and are mainly located in the western part of China. For data after 1961, missing values are rare for all stations. Further, a rapid increase in the number of observational stations is found from 1951 to 1961, after which time the number of stations is found to stabilize between 600-700 (Figure 2.1b–1d). It should be noted that data coverage was quite inhomogeneous prior

to 1961 (see Figure 2.1) and therefore interpolation quality from 1951 to 1960 could be degraded.

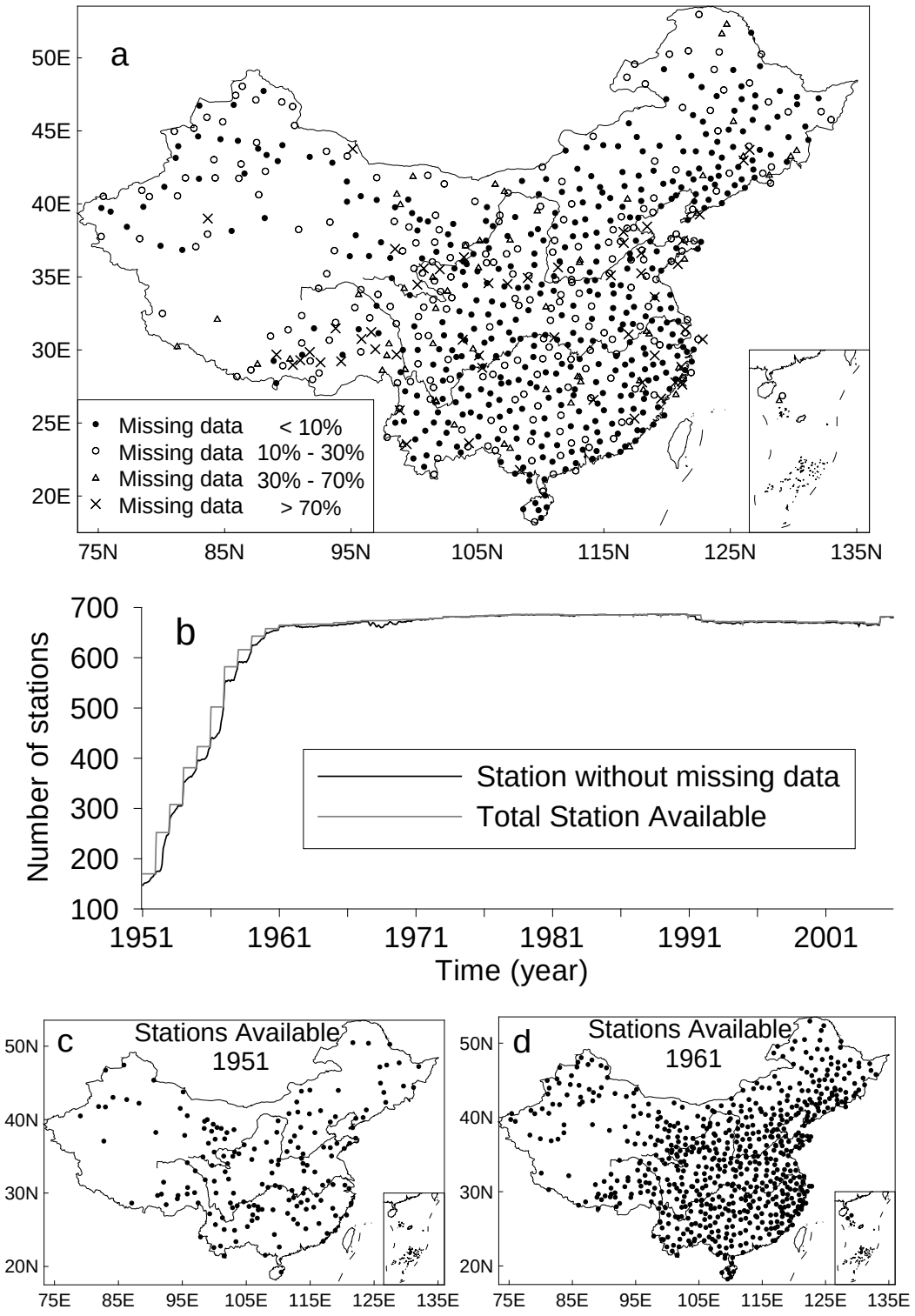

Figure 2.1 Location of the meteorological stations used in the work: a) all the 753 stations, b) number of stations in operation varies with time, c) stations operational from 1951 onward, and d) stations operational from 1961 onward.

Seasonal experimental semi-variograms were used to examine the variation in correlation between stations following the increase of the distance (Figure 2.2). The formula for semi-variograms is derived from that of variograms (Barnes 1991) which can be described as:

$$2\gamma(h) = E\{[Z(x) - Z(x+h)]^2\} \quad (2.1)$$

Then the semi-variogram is,

$$\gamma(h) = \frac{1}{2}E\{[Z(x) - Z(x+h)]^2\} \quad (2.2)$$

The experimental semi-variogram can be obtained as follows,

$$S = \frac{1}{2N}\sum_{i=1}^{N}(z(x_i) - z)^2 \quad (2.3)$$

where N denotes the set of pairs of observations between station i and the target station. An exponential model $r(h) = C(1 - e^{-h})$ was used to fit the experimental semi-variogram, where C is the scale of the semi-variogram and h is the relative separation/lag distance. The parameters for the four seasons were estimated separately: C=59 mm^{2}d^{-2}, h = 230 km for spring, C = 170 mm^{2}d^{-2}, h = 160 km for summer, C = 50 mm^{2}d^{-2}, h = 230 km for autumn, and C = mm^{2}d^{-2}, h = 350 km for winter.

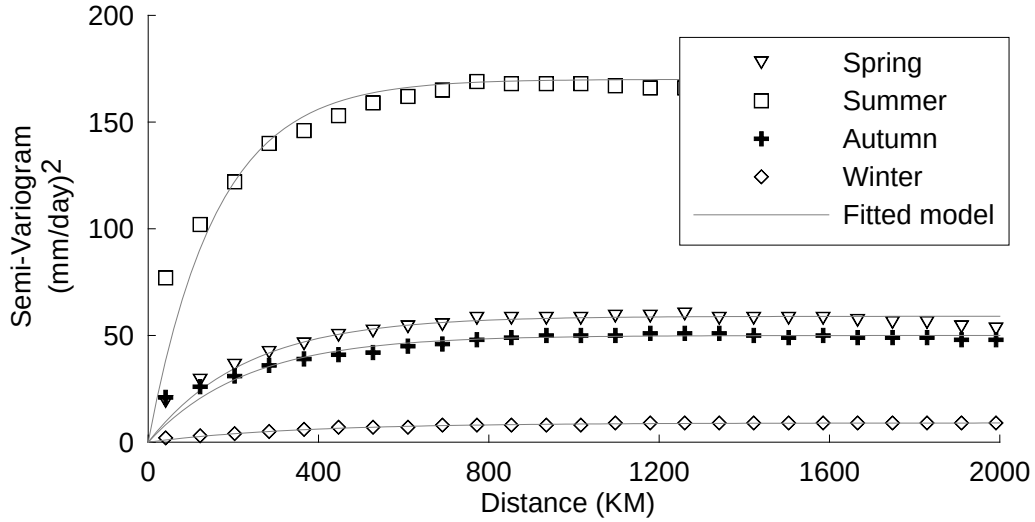

Figure 2.2 Seasonal Semi-Variogram.

It can be seen that the semi-variograms for spring and autumn are similar but those for winter and summer are substantially different. The highest values in summer indicate the dominating

summer monsoon in the region (Qian et al. 2003). The spatial correlation decreases with increasing precipitation. By contrast, the spatial precipitation distribution in winter is of large scale, while summer precipitation events are much more locally isolated. The semi-variogram models show that the correlation between stations decreases as the distance increases, and the correlation reaches a fairly constant level when the distance is around 800 km.

Finally, the data was interpolated onto a 18 km× 18 km grid system covering the whole country using the ordinary kriging (Goovaerts 2000). The daily precipitation for each 0.5x0.5^{o} latitude-longitude block was then obtained by averaging the values at the grid nodes within the block from 1951 to 2005 (Chen et al. 2010). This daily gridded precipitation dataset is freely available at http://rcg.gvc.gu.se/dc/.

2.1.2 Daily temperature

By using the same instrumental observational dataset introduced above, Xu et al. (2009) interpolated the daily mean temperature and daily minimum temperature onto a 0.5x0.5^{o} spatial resolution. In their work, stations with more than 1/3 (10 years) of their data missing were excluded from the analysis. The total number of stations included in their final calculations was slightly different from day to day, but was in the range of 654-662. A coarser resolution (1x1^{o}) version of this dataset is freely available at http://ncc.cma.gov.cn/Website/index.php?ChannelID=112 & WCHID=110. In this work, the daily 1x1^{o} mean temperature (TM) and minimum temperature (Tmin) dataset was used to define winter cold surges in southeast China.

2.2 Other gridded sea level pressure and temperature observations

Two observational gridded datasets: the Hadley Centre sea level pressure (SLP) (HadSLP2; Allan and Ansell 2006) and the National Centre for Atmospheric Research SLP (NCARSLP; Trenberth and Paolino 1980) were used to calculate the Siberian High intensity (SHI, the mean SLP within the region [40-65N, 80-120E]). The *in-situ* SLP observations from 20 stations located in the central SH region [40-65N, 80-120E], the same stations used by Panagiotopoulos et al. (2005), compiled by NCAR (available at http://dss.ucar.edu/datasets/ds570.0/), was also used to calculate the observed SHI.

Mean monthly surface temperature interpolated from station data to a 0.5x0.5^{o} spatial resolution grid from the Climatic Research Unit (CRU) at the University of East Anglia (New et al. 1999), was used to illustrate the winter (DJF) mean temperatures.

2.3 Reanalysis and CMIP5 simulations

2.3.1 Reanalysis

Daily precipitation from National Centers for Environmental Prediction (NCEP) and the National Center for Atmospheric Research (NCAR) reanalysis I (Kalnay et al. 1996) and European Centre for Medium-Range Weather Forecasts (ECMWF) 40-year re-analysis (ERA40) (Uppala et al. 2005) were used as references in the observation-simulation comparison of extreme precipitation. Monthly mean SLPs from the two reanalysis datasets were also used to calculate the SHI. Daily and monthly SLP and geopotential height (HGT) on pressure levels from NCEP/NCAR reanalysis I (Kalnay et al. 1996) were used to investigate the daily and seasonal (winter) atmospheric circulation related to cold surges.

2.3.2 CMIP5

The Coupled Model Intercomparison Project (CMIP) was established under the World Climate Research Programme's (WCRP) Working Group on Coupled Modelling (WGCM) as a standard experimental protocol for studying the output of coupled atmosphere-ocean general circulation models (AOGCMs). The CMIP provides a community-based infrastructure in support of climate model diagnosis, validation, intercomparison, documentation and data access. The research based on the dataset from phase three of the CMIP (CMIP3) (Meehl et al. 2007), provided much of the material for the Intergovernmental Panel on Climate Change (IPCC) Fourth Assessment Report (AR4; IPCC 2007).

The fifth phase of the CMIP (CMIP5) experiments addresses outstanding scientific questions that arose during preparation of the IPCC AR4 (Taylor et al. 2012). There are mainly three groups of simulations in CMIP5 based on the major purposes of the simulations: one group for evaluation and the other two for projections and feedbacks. The historical ensemble simulations, which were used in this work, are evaluation simulations that include all possible climate forcings. This is used to better characterize projected climate change and, more generally, to separate

signal from noise (Taylor et al. 2012). Due to the fact that CMIP5 is still in progress, daily precipitation data from 1961 to 2000 are only available from 21 CMIP5 global climate models, which were used to examine the simulated extreme precipitation in this study. Detailed information about the models can be found in Table 2.1.

Table 2.1 Model horizontal resolution (longitude x latitude in degree) of the 21 CMIP5 global climate models used

Model	Institute/Country	Atmosphere Resolution
MIROC4h	MIROC/Japan	0.5625x0.5616
CCSM4	NCAR/USA	1.2500x0.9424
MRI-CGCM3	MRI/Japan	1.1250x1.1215
CNRM-CM5	CNRM/France	1.4063x1.4008
MIROC5	MIROC/Japan	1.4063x1.4008
HadGEM2-ES	MOHC/UK	1.8750x1.2500
HadGEM2-CC	MOHC/UK	1.8750x1.2500
INM-CM4	INM/Russia	2.0000x1.5000
IPSL-CM5A-MR	IPSL/France	2.5000x1.2676
CSIRO-Mk3.6.0	CSIRO/Australia	1.8750x1.8653
MPI-ESM-LR	MPI-M/Germany	1.8750x1.8653
FGOALS-s2	IAP/China	2.8125x1.6590
NorESM1-M	NCC/Norway	2.5000x1.8947
GFDL-CM3	NOAA/USA	2.5000x2.0000
GFDL-ESM2G	NOAA/USA	2.5000x2.0225
IPSL-CM5A-LR	IPSL/France	3.7500x1.8947
MIROC-ESM-CHEM	MIROC/Japan	2.8125x2.7906
MIROC-ESM	MIROC/Japan	2.8125x2.7906
CanCM4	CCCMA/Canada	2.8125x2.7906
BCC-CSM1.1	BCC/China	2.8125x2.7906
HadCM3	MOHC/UK	3.7500x2.5000

3. Observed and simulated changes in extreme precipitation in China from 1961 to 2000

3.1 Observed change in extreme precipitation

3.1.1 The extreme precipitation indices used

Extreme precipitation can be represented by many different indices. Here, we choose 10 precipitation indices previously used by Alexander et al. (2006) and Moberg et al. (2006), which are shown and defined in Table 3.1. Two of the ten indices, namely the simple daily intensity index (SDII) and the annual total wet-day precipitation (PRCPTOT), are indices for average conditions; but a difference in the trend of SDII and PRCPTOT may reflect changes in the character of precipitation (Moberg et al. 2006), which may help to explain the variation of extreme precipitation. By checking this we may test a GCM performance in simulating extreme precipitation. Here, all the indices used are called extreme indices for the sake of simplicity. We use daily observations from 592 out of the 753 stations in China, i.e. those containing less than 1 year of missing values, between 1961 and 2000.

Two versions of gridded extreme precipitation indices were calculated based on EI_{STA} and EI_{GRID} respectively. For EI_{STA}, the selected indices were calculated for each of the 592 stations, then the resulting indices were interpolated onto a 0.5x0.5º grid using the inverse distance (power 2) method (Franke 1982). For EI_{GRID}, the extreme indices were directly calculated from the interpolated daily gridded precipitation.

3.1.2 Scaling effect on gridded extreme precipitation indices

Before examining the long-term change of extreme precipitation and evaluating the model simulations, the scaling effect on the extreme precipitation indices was examined for the two versions of gridded extreme indices (i.e. EI_{STA} and EI_{GRID}). Figure 3.1 shows the difference between the two versions of gridded indices depending on grid-cell size in 8 different resolutions (from 0.5x0.5º to 4x4º). Compared to the gridded indices from EI_{STA}, all indices from EI_{GRID}, except CDD and consecutive wet days (CWD), have decreased linearly with the increase in grid-cell size. The difference between extreme precipitation indices from EI_{STA} and EI_{GRID} is quite

large, especially for larger gird-cells (lower horizontal resolution). Taking the interpretation of model precipitation output as an area mean, it is better to use the indices based on EI_{GRID} to evaluate the model simulated extreme indices as suggested by (Chen and Knutson 2008). Consequently, the gridded extreme precipitation indices based on EI_{GRID} was used to evaluate model simulated extreme precipitation.

Table 3.1 Definition of the 10 precipitation indices used (most of them indicate extreme precipitation conditions)

CDD	Maximum length of dry spell, maximum number of consecutive days with precipitation (R) <1mm/day
CWD	Maximum length of wet spell, maximum number of consecutive days with R≥1mm/day
R10mm	Annual count of days when R≥ 10mm/day
R20mm	Annual count of days when R≥ 20mm/day
R95pTOT	Amount of precipitation in very wet days precipitation ($R95pTOT=\sum R$, where R>R95 (R95 is the 95th percentile of precipitation on wet days in the 1961-1990 period))
R99pTOT	Amount of precipitation in extremely wet days ($R99pTOT=\sum R$, where R>R99 (R99 is the 99th percentile of precipitation on wet days in the 1961-1990 period))
Rx1day	Maximum 1-day precipitation amount
Rx5day	Maximum consecutive 5-day precipitation amount
PRCPTOT	Annual total wet-day precipitation ($PRCPTOT=\sum R$)
SDII	Simple daily intensity index ($SDII=PRCPTOT/WD$, WD is the total number of wet days (R≥1mm/day))

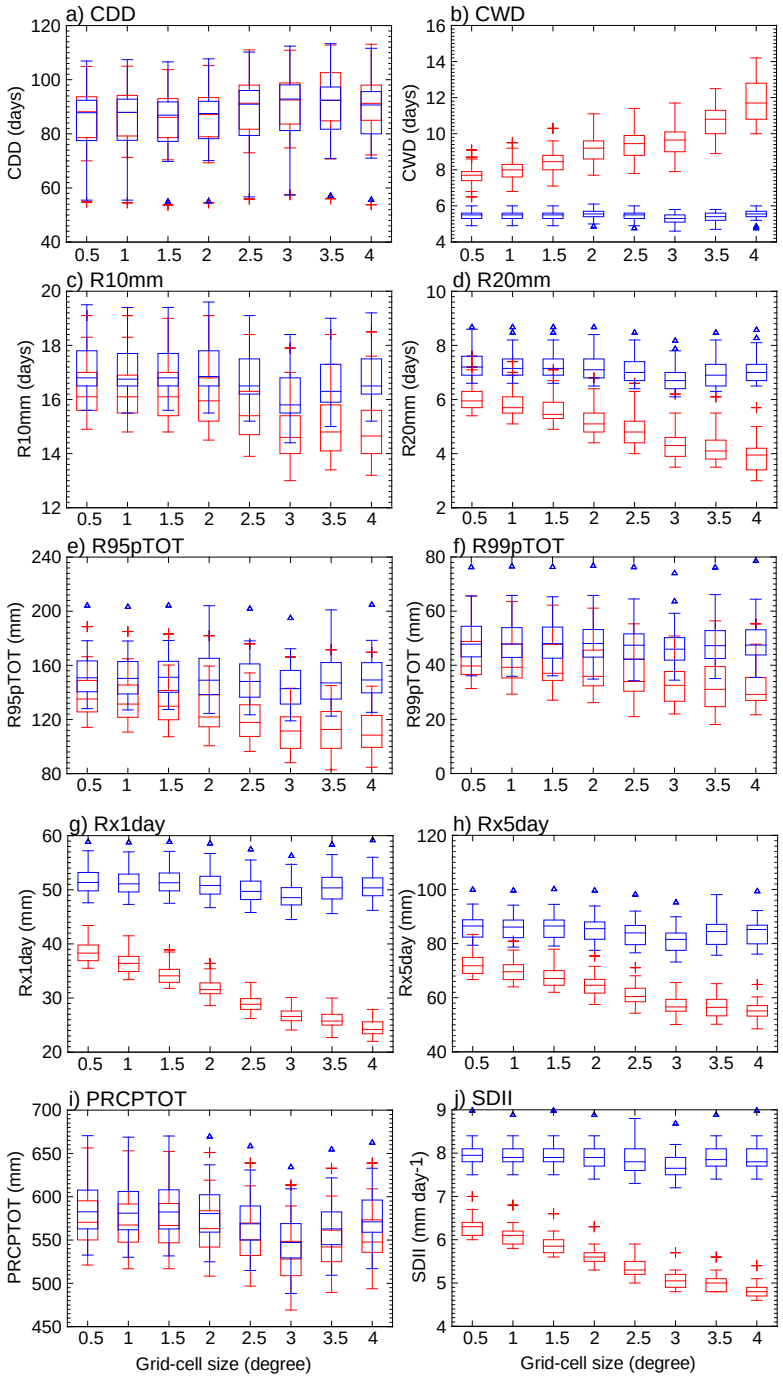

Figure 3.1 Comparing between extreme indices based on EI_{STA} (Blue) and EI_{GRID} (Red) over Mainland China with 8 different horizontal resolutions (0.5x0.5, 1x1, 1.5x1.5, 2x2, 2.5x2.5, 3x3, 3.5x3.5, and 4x4 degree) for 10 indices (a-j). Box-Whisker Plot shows the statistic characteristic of the selected index at the selected resolution during 1961-2000, the lower, middle and upper line of the box show the lower quartile (Q1, QL is the value of Q1), median (Q2), upper quartile (Q3, QU is the value of Q3) respectively, the ends of the whiskers shows the lowest datum still within 1.5 interquartile range (IQR, IQR=QU-QL) of the Q1, and the highest datum still within 1.5 IQR of the Q3, data fall below QL-1.5_xIQR or above QU-1.5_xIQR have been shown as outliers.

3.1.3 Observed long-term trends

When evaluating model simulated extreme precipitation, the observed linear trend was also examined using the indices from EI_{GRID}. The linear trends of 10 precipitation indices on 2.5x2.5^{o} resolution were examined, the reason for the selection of this resolution being that most of the models and the reanalysis data sets have a resolution of around 2.5x2.5^{o}. Results show that the spatial pattern of the linear trends is generally the same for all the selected extreme precipitation indices, except for CDD (Figure 3.2). Here, only the spatial patterns of the amount of precipitation on very wet days (R95pTOT), one widely used extreme precipitation index, and CDD are discussed.

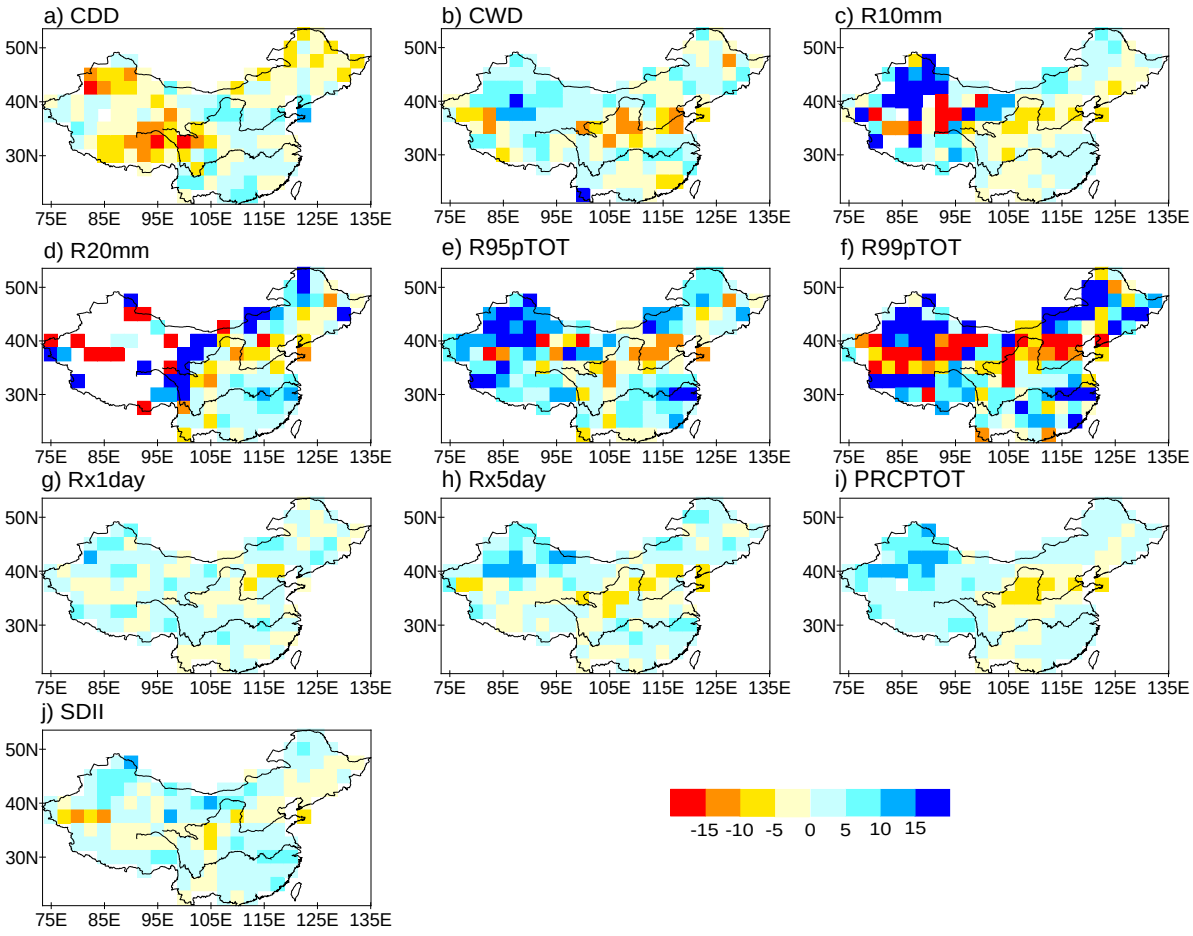

Figure 3.2 Linear trend of 10 observed extreme precipitation indices during 1961-2000 (spatial resolution 2.5x2.5^{o}) (Units: % per 10 year)

From 1961 to 2000, the observed R95pTOT increased in most parts of China, with the exception of northern China (Figure 3.2e). This difference in trends of extreme precipitation for northern and southern China have previously been mentioned by Zhai et al. (2005) and Qian et al. (2007a), where it is noted that the precipitation decrease in northern China and increase in southern China, especially along the Yangtze River valley, may be due to the weakening trend of the East Asian summer monsoon (EASM) (Qian et al. 2007a).

The spatial pattern of the linear trends of CDD is clearly illustrated by the first Empirical Orthogonal Function pattern of CDD from 1961 to 2000 (Xu et al. 2011). The observed CDD shows decreasing trends in northwest and northeast China and an increasing trend in eastern China from 1961 to 2000. Generally, the observed linear trend of CDD is opposite to the trend of R95pTOT (Figure 3.2a, e), but in southeast China, both R95pTOT and CDD increased from 1961 to 2000.

3.2 Simulated change in extreme precipitation

The simulated extreme precipitation over China was evaluated by considering the scaling effect (Figure 3.3), that is using EI_{GRID} indices with the same horizontal resolution of the target model. Regarding the reanalysis datasets, the extreme indices from ERA40 generally agree better with the observations compared with those from NCEP, which is in agreement with the findings of Ma et al. (2009). Turning to the climate models, the climatological mean of CDD from 1961 to 2000 is generally underestimated, and that of CWD is overestimated (Figure 3.3a, b). The R10mm days, R95pTOT and R99TOT, are generally overestimated (Figure 3.3c, e, f), while the simulated R20mm days are closer to observations (Figure 3.3d). These results indicate that the climate models tend to overestimate the number of wet days, especially those with moderate precipitation rates. Further, Rx1day and Rx5day precipitation are mostly overestimated (Figure 3.3g, h). Most of the models simulate SDII fairly well (Figure 3.3j), while PRCPTOT (Figure 3.3j) is largely overestimated. This indicates the models tend to simulate more precipitation days, coinciding with the overestimated CWD and underestimated CDD.

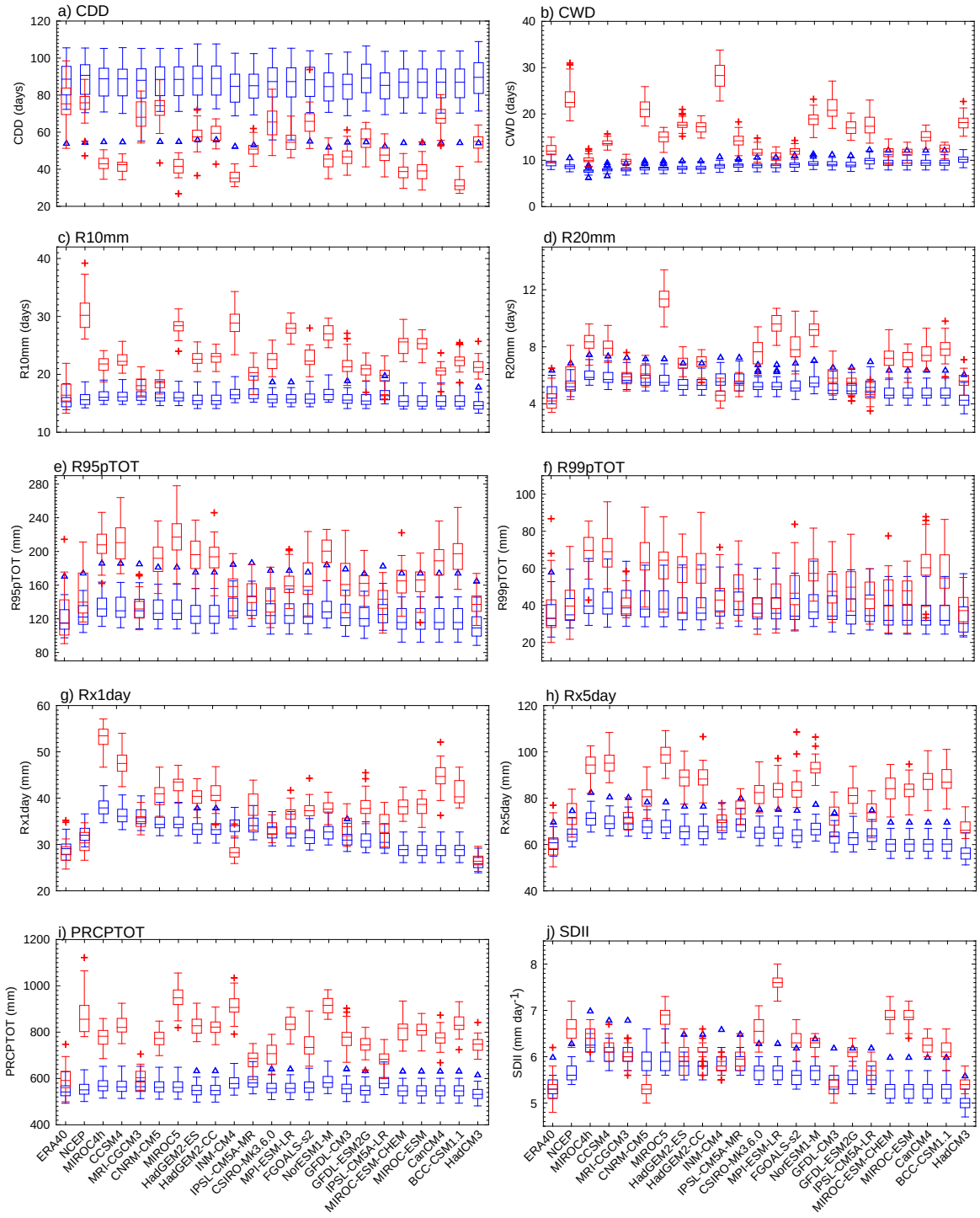

Figure 3.3 Comparing between extreme indices from 21 CMIP5 global climate models and two reanalysis (Red) and gridded observed index based on EI_{GRID} with the same resolution (Blue) over Mainland China (south of 21N is not counted) for 10 indices (a-j) during 1961-2000 (Same Box-Whisker Plot as in Figure 3.1 have been used).

The simulated spatial patterns of most indices are similar to PRCPTOT except for CDD. Therefore we hereafter only focus on the spatial patterns of PRCPTOT and CDD. Most of the models overestimate PRCPTOT and underestimate CDD in the western and northern regions of China (map not shown), but underestimate PRCPTOT and overestimate CDD in southeast China. The overestimated precipitation around the boundary region of the Tibetan Plateau seems be influenced by topography (Feng et al. 2011). The difference between simulated and observed R95pTOT in the Tarim and Jungar basins, both of which are located in western China, is difficult to explain, given that there are few, if any, observations available for these regions (Feng et al. 2011). The relatively poor performance of climate models in western China is most likely due to the low frequency of extreme precipitation and rain days occurring in this region as compared to eastern China (Fu et al. 2008).

The linear trends of R95pTOT and CDD are shown in Figure 3.4 and 3.5. The observed increasing trend of R95pTOT in northwest China is relatively well captured by most of the models but the trends in southeast and northern China are poorly reproduced (Figure 3.4). The simulated linear trend of CDD is, in general, opposite to the trend of R95pTOT in the study area, which is better fits observation. The observed trend of CDD and R95pTOT in southeast China is poorly reproduced by most of the models (Figure 3.5).

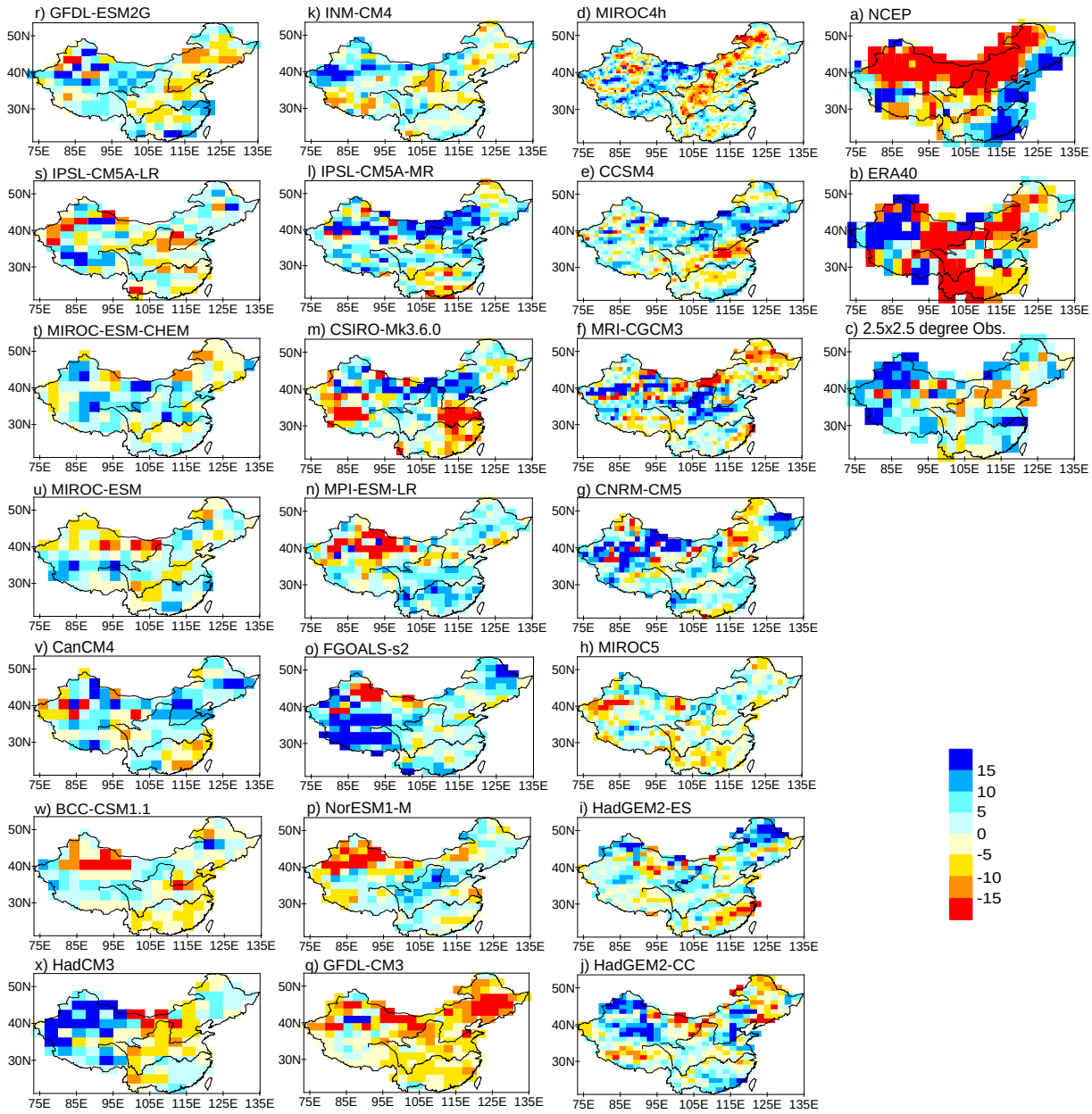

Figure 3.4 Spatial distribution of the linear trend of R95pTOT during 1961-2000 (units: % per 10 year) of two reanalysis (a, b), gridded observation based on EI_{GRID} on 2.5x2.5^{o} resolution (c) and 21 CMIP5 global climate models (d - x).

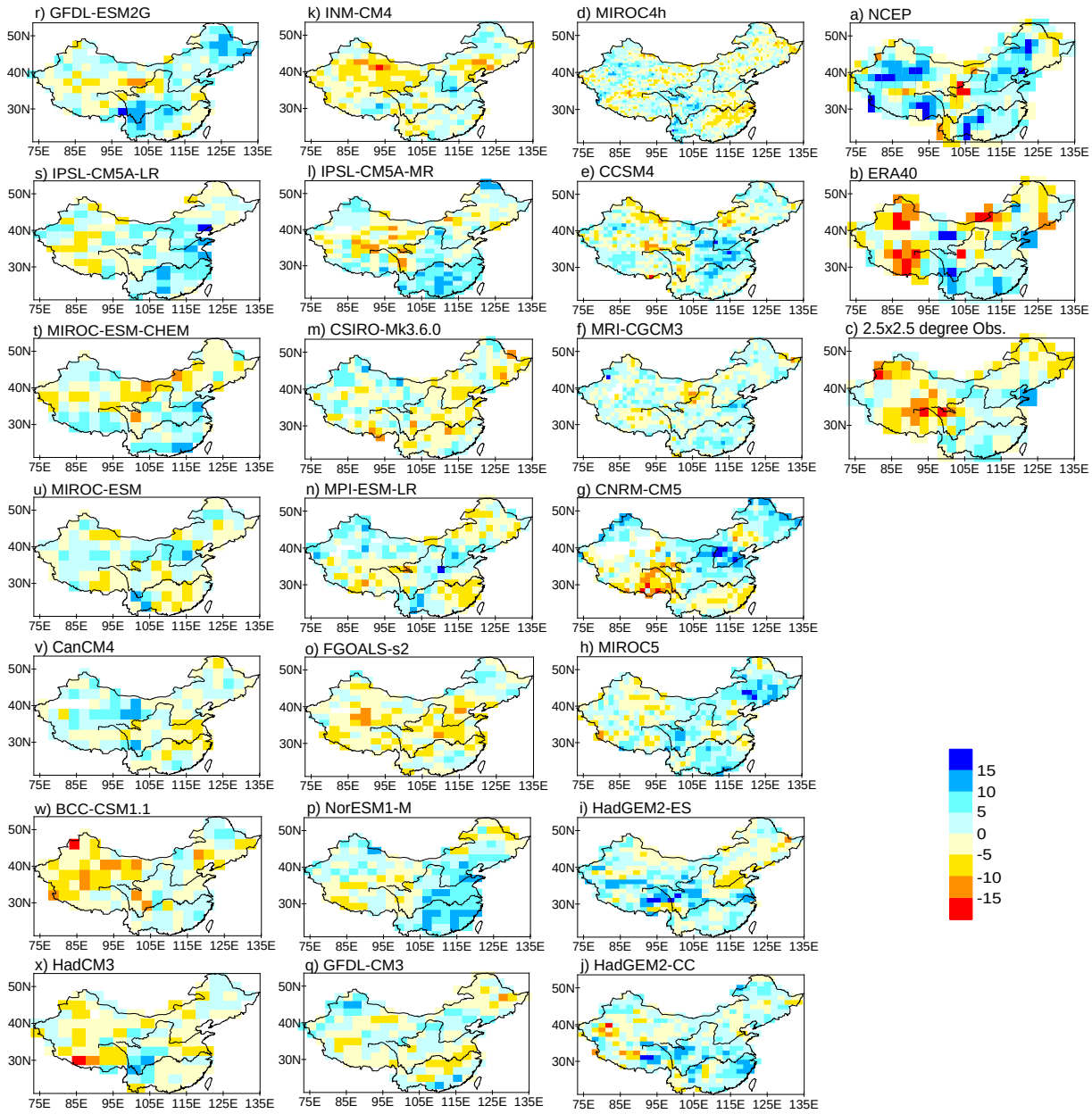

Figure 3.5 same as Figure 3.4, but for CDD.

4. Winter cold surges in southeast China and their relationship with atmospheric circulation patterns from 1961 to 2005

4.1 Climatology of cold surge occurrences

A sudden drop in daily temperature is one of the key indications of a cold surge outbreak, and previous studies have used this as a main criterion of cold surge detection (Wang and Ding 2006; Ding et al. 2009). Considering the definition of regional cold surges used by Wang and Ding (2006), we use temperature drop thresholds in daily TM to determine the occurrences in southeast China; a cold surge event is indicated if least 10 (out of 121) $1x1^{o}$ grid boxes satisfy both the following criteria:

a) The daily TM drops more than $6^{o}C$ within 24-48 hours
b) The TM anomaly is less than $-3^{o}C$, and the daily Tmin is less than $15^{o}C$

Using the definition above, 175 cold surges were identified in winter (DJF) between 1961 and 2005 in southeast China: an average of 4 per year.

4.2 Siberian High and its impacts on cold surge occurrences

Wang and Ding (2006) point out that the occurrence of winter cold surges in China is closely related to the Siberian High intensity (SHI: mean SLP in the region [40-65N, 80-120E]). In this work, the relationship between the SHI and the occurrence of winter cold surges in southeast China is investigated. First, the temporal variation of the SHI during the past 100 years is examined. Figure 4.1 presents the time series of the SHI from instrumental observations and reanalysis data sets. The most conspicuous feature during the 20th century is a steep declining SHI trend from the 1970s to 1990s, leading to record-low SHI values for most observational data sets in the early 1990s. Only the NCEP reanalysis data set shows a very weak trend during this period, but this is likely associated with the known systematic bias of the NCEP reanalysis in representing inter-decadal changes over the Eurasian continent (Wu et al. 2005), leading to an exaggerated cold period around 1972–1977 compared to other data sets. In the early to mid-1990s, however, the declining trend turned sharply positive, and the SHI records show a continuous recovery, reaching a climatologically normal state in recent years. The increased snow cover in

Eurasia in late fall (October-November) and winter may have led to the recovery of the SHI since the early 1990s (Jeong et al. 2011).

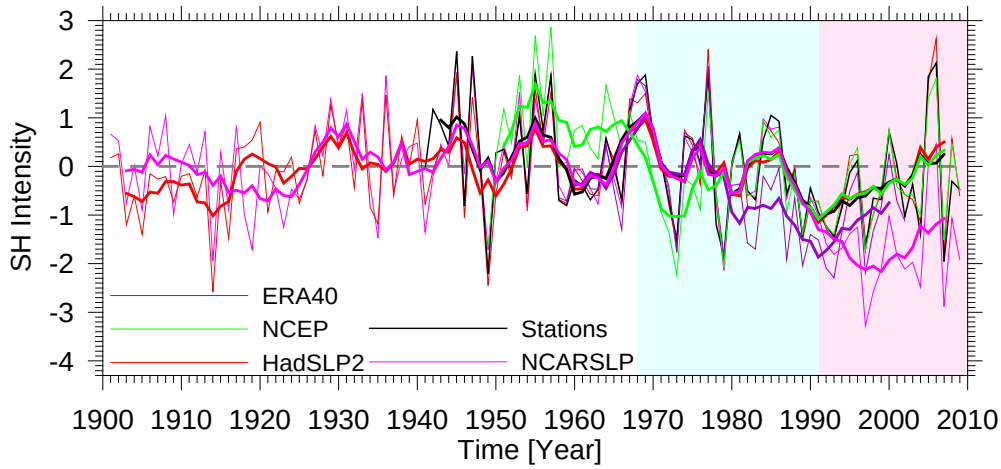

Figure 4.1 Time series of winter SHI derived from 5 SLP data sets from 1900 to 2009. Thick lines indicate 5-year running averaged time series. Each time series is standardized for the comparison with respect to the mean and standard deviation for 1958-1980 of each data set. The area with a background color of sky blue (pink) indicates the period of the SHI decline (incline) defined in the present study.

The SHI from NCEP reanalysis, which includes 3-dimensional data sets during the study periods, is used to examine the relationship between the SHI and the occurrence of cold surges. Note that the SHI from NCEP is weaker than the other data sets during the period around 1970. The time variation of the SHI and the cold surge occurrence in winter are shown in Figure 4.2. It is clearly found that inter-annual and inter-decadal variation in the occurrence of cold surges follows well the SHI variation. From the 1960s to the early 1970s, the occurrence of cold surges significantly decreased. Another prominent decrease in both records is found during 1980s, reaching its minimum in the early 1990s. After the mid-1990s, the number of cold surge has remained stable, with annual occurrences of 3-4. The annual occurrence is significantly correlated with winter mean SHI (the correlation coefficient is 0.4, which is significant at the 0.01 level), and there is an even closer correlation in the low frequency variation between the two. As indicated by Zhang et al. (1997), the cold surge frequency may not monotonically increase as the SH intensifies. Some weaker SH years could also produce a high frequency of cold surges. To understand the relationship between the SHI and the occurrence of the cold surges, the next step is to examine the daily and seasonal (winter) atmospheric circulation patterns related to cold surges.

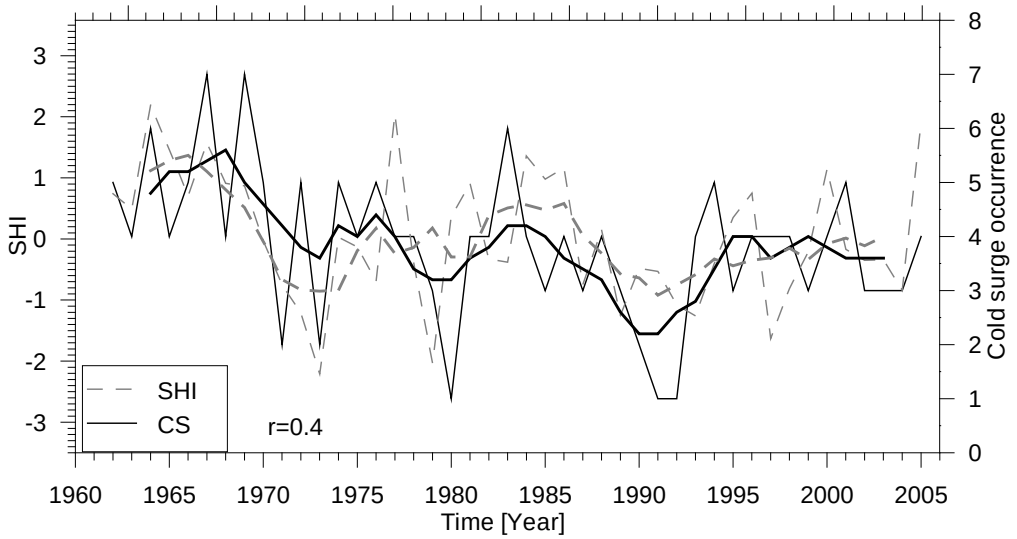

Figure 4.2 Time series of the occurrence of the winter (DJF) cold surges (CS) in southeast China and SHI (thick lines indicate 5-year running average)

4.3 Relationship between the occurrence of cold surges and circulation changes

4.3.1 Circulation patterns related to different cold surge groups

In order to understand the link between atmospheric circulation patterns (e.g., the SH) and the occurrence of cold surges, we first analysed the daily atmospheric circulation patterns related to cold surges. Daily SLP fields were studied over the region (indicated by Figure 1.1) from 9 days prior to until the day of the outbreak of a cold surge for all the identified cold surge events. The cold surges were subjectively divided into 5 different groups based on the different day-to-day evolution of high pressure systems over the northern central Eurasian continent (i.e., central Siberia) related to the cold surges:

A. A stationary high pressure system located in the Siberian region (33.1%, including two subgroups)

   A1. No clear movement of the center of the SH (31 cases)

   A2. Moving center of the SH (27 cases)

B. A Moving high pressure from the west to the Siberian region (40.0%, including two subgroups)

   B1. The SH is replaced by a high pressure moving in from the west (43 cases)

B2. The SH is merged with a high pressure moving in from the west (27 cases)

C. Blocking in the Ural Mountains region (11.4%, including two subgroups)
   C1. A blocking high occupies the Ural regions until the outbreak of a cold surge (16 cases)
   C2. Initial blocking high in the Ural regions moves into the Siberian region within 5 days of a cold surge outbreak (4 cases)

D. A high pressure moving from the northern Arctic region into the Siberian region (13.1%, 23 cases)

E. A strong low pressure system moving to the northwest of the Siberian region 3 days prior to the cold surge outbreak (2.2%, 4 cases, will not be discussed in this work)

The composite SLP maps for the day 6 days prior to the outbreak of a cold surge (day -6), day -3 and day 0 (the day of outbreak) are shown in Figure 4.3. From the Figure 4.3 we can see that a significant TM drop (more than 6^{o}C) is found over southeast China on day 0 for all groups except A.

In both subgroups A1 and A2, there is a high pressure system located in the Siberian region 6 days prior to the cold surge outbreak (Figure 4.3). The high pressures in group A1 are stronger than those in group A2, and the centers (area with SLP larger than 1030hPa) of the high pressure systems in group A1 are larger than those in group A2. At 500hPa, there is a positive HGT anomaly over the northern part of the Siberian region which forms on day -6 and lasts until the outbreak of a cold surge in group A (Figure 4.4).

In the group B events, 6 days prior to the outbreak of a cold surge, the high pressure in the Siberian region is relatively weak compared to group A (Figure 4.3). The high pressure is then strengthened by a high pressure system moving from the west into the Siberian region 3 days prior to the outbreak, and subsequently the high pressure expands into southeast China, bringing cold air to this region, i.e., causing a cold surge outbreak. More areas exhibit temperature drops larger than 6^{o}C in group B than in group A. During group B events there is a pattern of HGT anomaly at 500hPa that is opposite patterns for group A events 6 days prior the outbreak of a cold surge. Then the signal moves eastwards, which may lead to the eastward movement of the high pressure at lower levels (Figure 4.4).

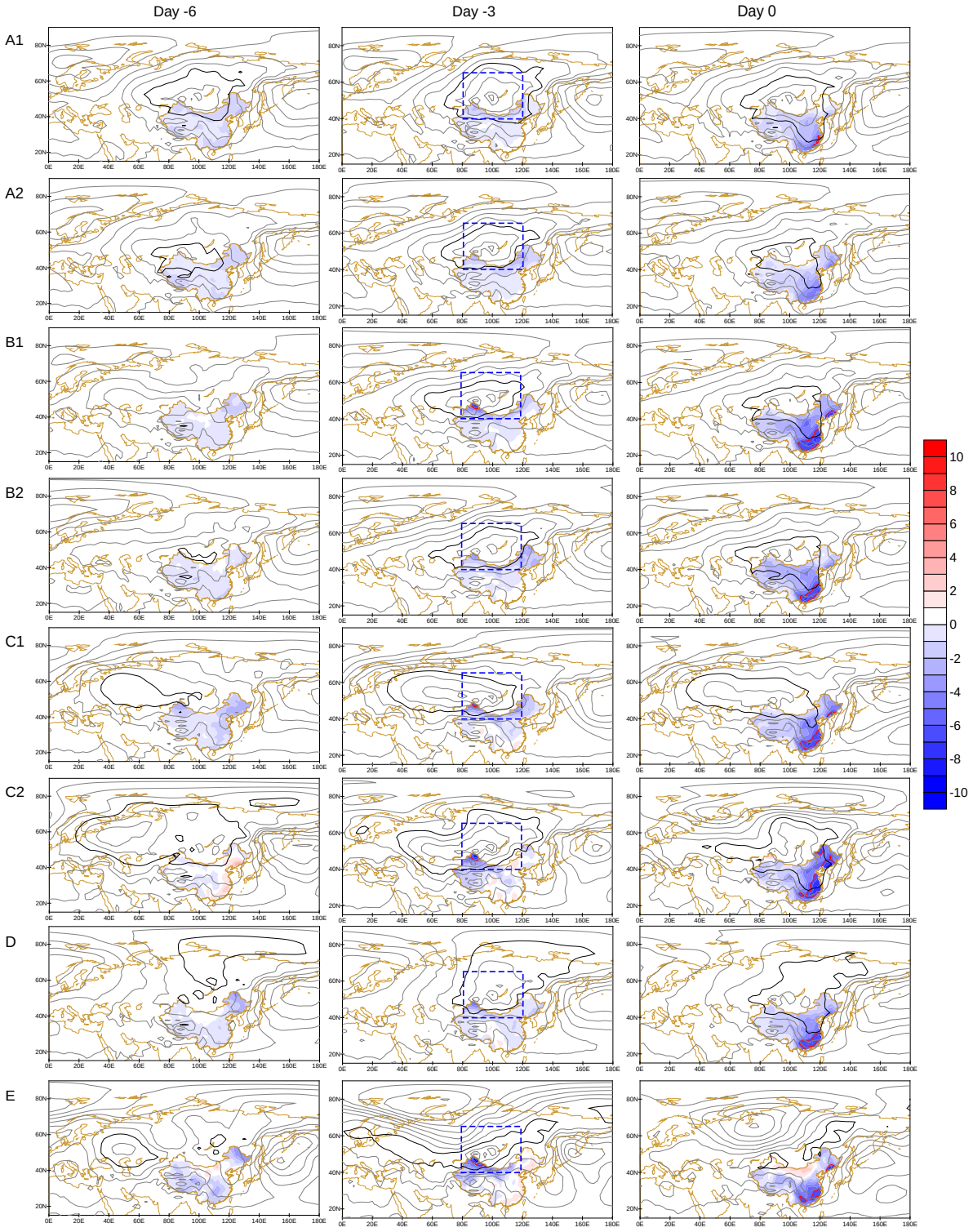

Figure 4.3 Composite maps of SLP (contours, intervals 5hPa) and maximum TM drop (shaded) within 24-48 hours on day -6, day -3 (- indicates the day before the outbreak of a cold surge), and day 0 (outbreak day of a cold surge) according to the cold surge day (day 0) for 8 different groups (black line indicate the contour line of 1030hPa, red lines indicate the TM drop 6^{o}C, dashed blue square on day -3 indicate the region to calculate the SHI)

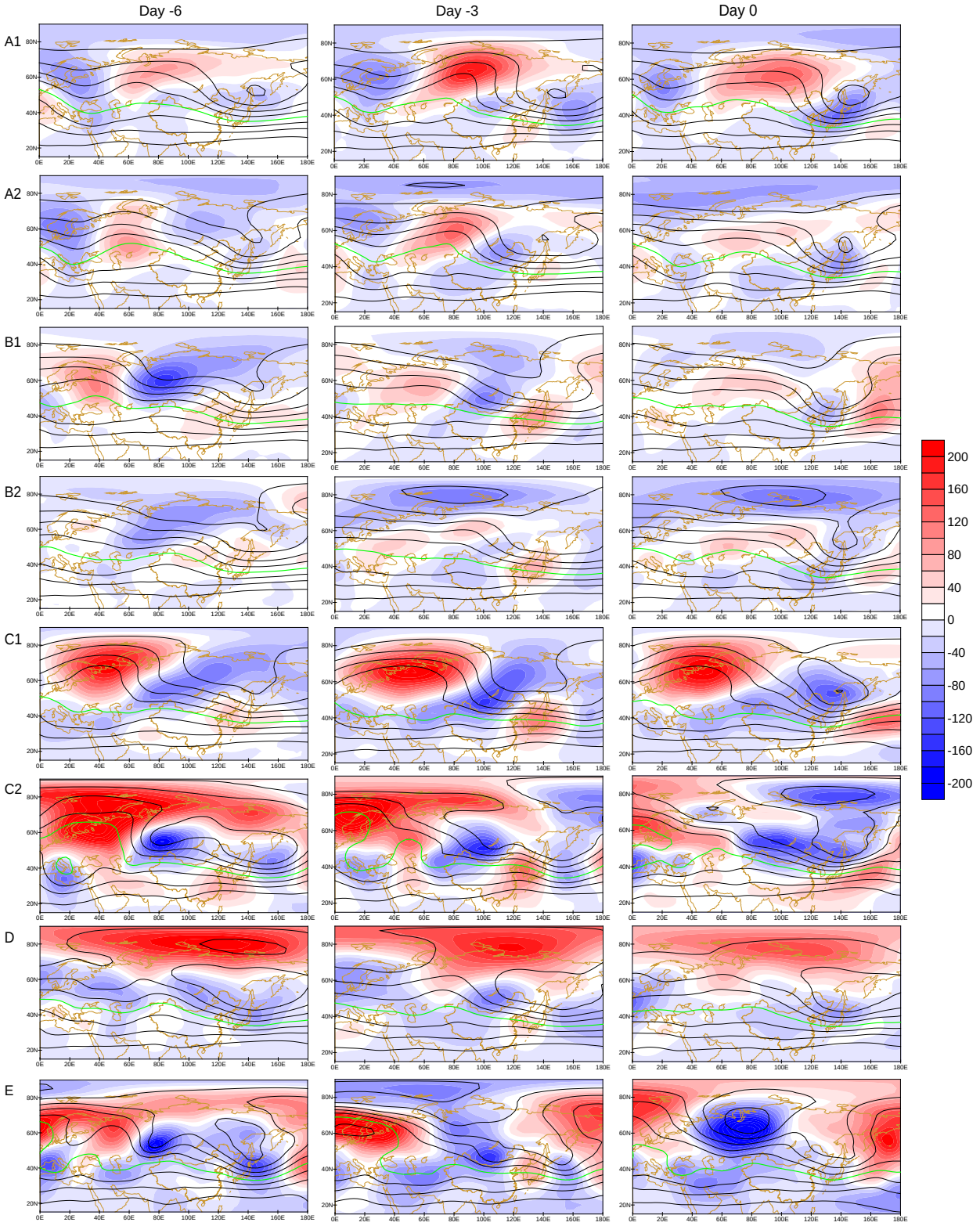

Figure 4.4 Same as Figure 4.3, but for composite maps of HGT (contours, intervals 100m, green line indicate the contour line of 5500m) and HGT anomaly (shaded) at 500hPa

During the group C events, there is a blocking high located around the Ural Mountains region 6 days prior the cold surge outbreak (Figure 4.3). The eastern part of this high expands first into the Siberian region and then into southeast China in group C1 events. During group C2 events, the eastern part of the high moves into the Siberian region and the west part of the blocking slowly follows within 5 days of the cold surge outbreak. The blocking pattern around the Ural Mountains can be seen in the mean HGT at 500hPa (Figure 4.4).

In group D events, a high pressure is located in northern Eurasia and the adjacent Arctic region close to the Far East 6 days prior to a cold surge outbreak, and then the high pressure slowly moves southwards and expands into southeast China, bringing cold air into the region (Figure 4.3). There is a positive HGT anomaly located in the Arctic region at 500hPa during group D events (Figure 4.4).

In group E events, one cyclone generates in the Arctic region and moves to the Ural Mountains region 3 days prior to the outbreak (Figure 4.3). The cyclone moves to the northwest of the Siberian region and pushes the high pressure southeastward, causing cold air to flow into southeast China and consequently generating a cold surge.

The cold surges of group A seem to behave quite differently from those of the other groups. The mean SHI from day -3 to day -1 is relatively strong, especially for group A1 events, but their impact area (the area in which there is a TM drop of more than 6^{o}C during a cold surge outbreak) is relatively small (Figure 4.5). This indicates that strong cold surge events (i.e. those affecting large areas) in southeast China are not directly linked to strong high pressure in the Siberian region.

In the works of Park et al. (2008; 2011a) cold surges in East Asia were divided into two types on the basis of origination: wave train types and blocking types. The upper level atmospheric circulation pattern of the blocking type is similar to that of group D in our work. These cold surges often occur in association with a negative phase of Arctic Oscillation (AO). The contribution of group D events to the total number of winter cold surges since 1980 is relatively small (Figure not shown). In the A, B and C groups, there are clear wave train patterns in the upper level, similar to those shown by Park et al. (2011a). Nevertheless, the more detailed subgrouping in this work makes it possible to identify distinctive upper level circulation patterns

related to cold surges, which may improve our understanding in the impact of the atmospheric circulation on cold surges in southeast China.

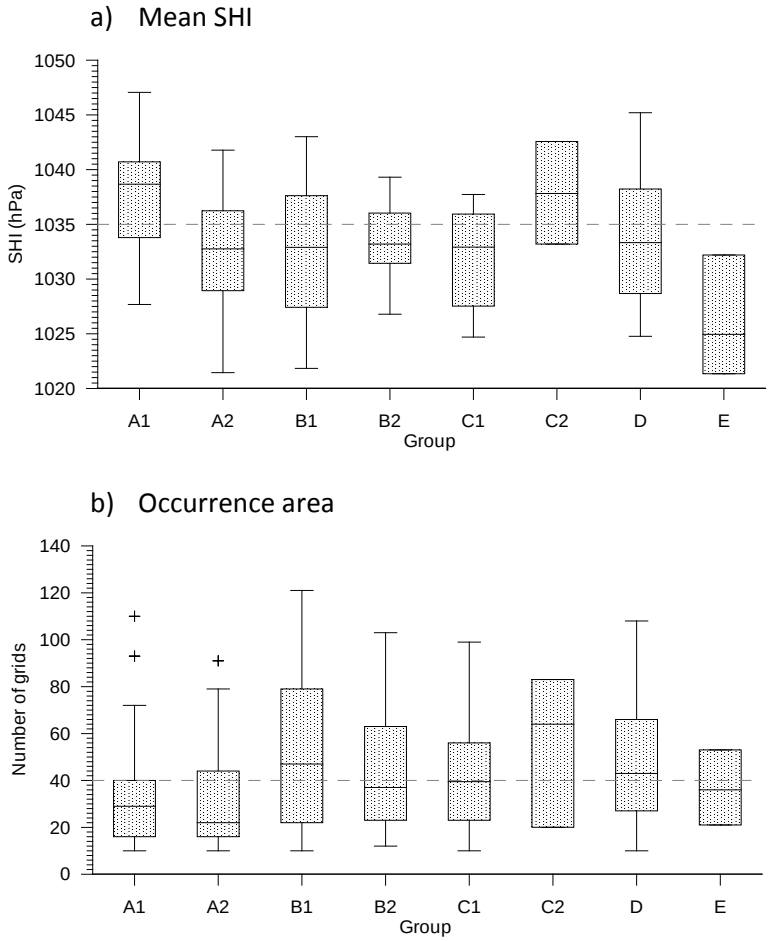

Figure 4.5 Box-whisker plot of a) mean SHI (in hPa) during 3 to 1 day prior to a cold surge outbreak and b) the impact area of the cold surge (number of grids which there is a TM drop of more than 6^{o}C during a cold surge outbreak) for 8 different subgroups

4.3.2 Change in the occurrence of cold surges

Going back to the relationship between the SHI and the occurrence of cold surges, the relationship seems clearer when looking at the variation in the occurrences of cold surges in different groups (Figure 4.6). We can see that the occurrence of cold surges in group A is highly coherent with the variation of the SHI (the correlation coefficient is 0.32 which is significant at the 0.05 level); a more positive SHI is associated with more occurrences of cold surges of group A. However, the occurrences of cold surges in groups B and C are seemingly not significantly

influenced by the variation of the SHI (the correlation coefficient is 0.13 and -0.04 respectively). In fact, the occurrences of cold surges in groups B and C increased after 1980 (Figure 4.6).

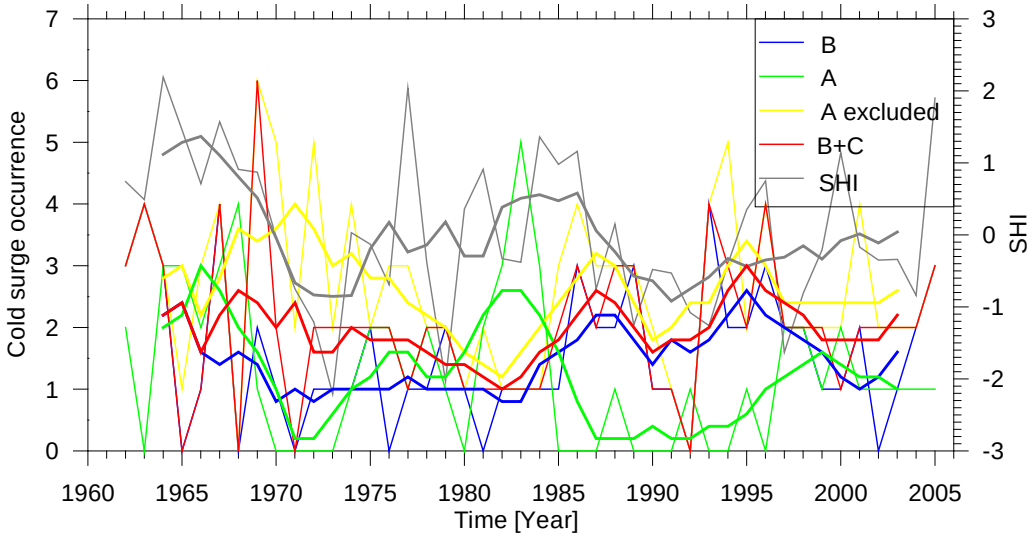

Figure 4.6 Annual occurrences of clod surges related to different combination of cold surge groups and the SHI (thick lines indicate 5-year running average)

5. Discussion

5.1 Model simulated trends of extreme precipitation

The increasing trend of extreme precipitation in western China is relatively well captured by most of the analysed models. As pointed out by Gao et al. (2002), the number of rain days in northwest China will significantly increase under global warming, and possibly this is the case for most of western China. However, when it comes to eastern China, where weather and climate are strongly influenced by the East Asian Monsoon System (Ding and Chan 2005; Qian and Lee 2000), the difference in trends of extreme precipitation in its northern and southern regions (Qian et al. 2007a; Zhai et al. 2005) is poorly reproduced. This may be due to the poorly captured inter-annual and inter-decadal variation of the summer monsoon in this region by the models, as illustrated by Gu and Li (2010).

The EASM has weakened since the end of the 1970's (Wang 2001; Yu et al. 2004). Associated with this weakening, precipitation decreased in northern China, but increased over the middle and lower reaches of the Yangtze River valley (Hu et al. 2003; Yu and Zhou 2007; Yu et al. 2004). This has led to a decrease of extreme precipitation in northern China and an increase in southern China, especially along the Yangtze River valley (Qian et al. 2007a). As pointed out by Zhou et al. (2009), the East Asian summer monsoon has the lowest reproducibility and is the most poorly modelled of the monsoon subsystems around the globe. The reason is mainly due to the model's bias in simulating sea surface temperature (SST) patterns and associated land-sea thermal contrast change across the East Asia (Zhou et al. 2009). Some other external factors like the remote influences of summer North Atlantic Oscillation (SNAO) (Linderholm et al. 2011) also need more attention in order to better simulate precipitation extremes over the East Asia.

The ESWM has significantly weakened since the late 1980s (Wang et al. 2009), more specifically after around 1986 (Wang and Chen 2010). This could lead to fewer rain days and additional dry days during the winter season, especially in southern China where there the CDD has significantly decreased, as illustrated by Wang and Yan (2009). Moreover, the significantly increased aerosol concentrations, produced by air pollution, may also have reduced the number of light rain events in eastern China (Qian et al. 2009). Thus, the combined effects of a weakening EAWM and an increase of aerosols could have combined to lead to the increase of CDD in

eastern China, such that CDD has increased in both southern and northern China, while extreme precipitation has increased in southern China but decreased in northern China. Monsoon variability (both of the EAWM and EASM) and the aerosol effect on precipitation should be accurately represented in global climate models in order to better simulate extreme precipitation in eastern China.

5.2 The occurrence of cold surges

The impact area of cold surges in group A is relatively small compared to that in other groups (Figure 4.5), and there are weaker TM drops in the composite map (Figure 4.3), especially for cold surges in group A2. This may be because the cold surges in group A occur mainly during strong SH years, in which surface temperature is usually lower than normal in east China (Gong and Ho 2002; Wu and Wang 2002). Since the temperature in southeast China will rarely drop more than 6^{o}C from the already low temperatures associated with the strong SH, the impact area of cold surge in group A will be relatively small. Conversely, looking at the circulation patterns of the other surge groups, the SH is relatively weak before the outbreak of a cold surge, which means that that air temperatures in southeast China will be normal (or higher than normal) before the outbreak of a cold surge. When the SH suddenly intensifies, cold air moves into southeast China following the southeastward expansion of the SH. This can lead to temperature drops of more than 6^{o}C in large areas, and this would explain why the impact areas of the cold surges in groups B-D are relatively large.

Cold surges in groups A and B are the two most common cold surge types, containing 58 and 70 cold surge events, respectively, out of the total of 175 cases. Since there are clear differences in the inter-decadal variability of cold surge occurrences between these two groups (Figure 4.6), it would be of interest to analyse whether this discrepancy can be related to differing responses during strong and weak SH years. The frequencies of annual cold surge occurrences for the two groups during strong and weak SH years for two different periods, 1961 to 1980 and 1981 to 2005, are shown in Figure 5.1. There is no clear change in the frequency of cold surges in group A and B between the two periods during strong SH years. However, during weak SH years, the frequency of cold surges in group B increased in the later period, while the change in group A was marginal. This is one main reason for the nearly unchanged frequency of cold surges in

southeast China in the later period, as surface air temperatures in China in the later period were in general higher than those of the former period (Liu et al. 2004) and the SH was relatively weak during most of this time (Figure 4.1). However, no clear decreasing trend in the occurrence of cold surges in southeast China could be identified despite the warming trend after 1980. Thus, although the SH may become weaker than normal in future warmer condition (Jeong et al. 2011), our results suggest that the occurrence of winter cold surges in southeast China, especially those with large impact areas such as the cold surges in group B, could remain unchanged in the future. This finding is in line with those obtained by Park et al. (2011b) who looked at could surges from future projections.

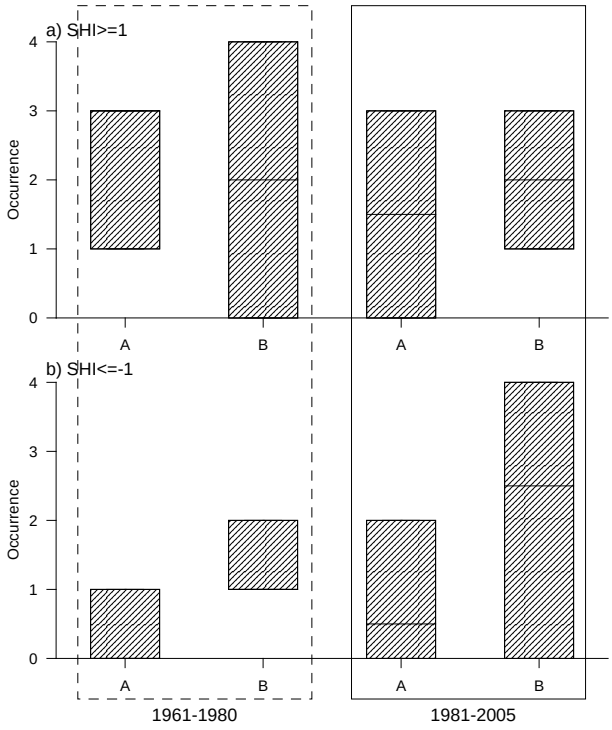

Figure 5.1 The frequency of annual cold surges in groups A and B during 1961-1980 and 1981-2005 under a) strong SH years (SHI≥1) and b) weak SH years (SHI≤-1)

So far, the circulation patterns related to cold surges have only been subjectively classified. An objective method is needed, through which changes in the frequency of the circulation patterns that may lead to the outbreak of cold surge can then be examined. This could improve our understanding of the mechanisms behind the occurrence of cold surges of different types, and possibly lead to better methods for the prediction of cold surge events. Moreover, it would shed some light on the projection into the future in the occurrence of cold surges in southeast China.

6. Conclusions

The following conclusions have been drawn:

a) The effects of two different methods for estimating extreme precipitation indices are significant. It is suggested that gridded extreme precipitation indices based on EI_{GRID} (estimation from a gridded precipitation dataset) should be used to evaluate model simulated precipitation extremes.
b) Most global climate models tend to overestimate extreme precipitation amounts but underestimate consecutive dry days, especially in mountainous regions. The pattern of extreme precipitation from 1961 to 2000 in western China is, in general, well captured by most of the models, while in eastern China it is poorly reproduced.
c) The occurrence of winter cold surges in southeast China significantly decreased between the 1960s and early 1970s, while the level of occurrence has been fairly stable since 1980, except for few years in the early 1990s.
d) The frequency of cold surges in group A, which have a small spatial impact in southeast China and are highly related to the variation of the winter mean SH, has decreased during the last 20 years, coinciding with a relatively weak SHI. On the other hand, the occurrences of cold surges in group B and C (51.4%), which have a larger spatial impact on the region, have increased since the early 1980s. This increase has compensated for the decrease of group A and D events, so that there is no clear decrease in the annual average occurrence of cold surges in southeast China after 1980. This indicates that the occurrence of the winter cold surges in southeast China, especially those with large impact areas, may not decrease in future.

Acknowledgements

I wish to express my gratitude to all the people at the Department of Earth Sciences, University of Gothenburg, who supported me throughout my Ph.D. thesis work. Above all, I want to send my thanks to Prof. Deliang Chen and Prof. Hans Linderholm who have been my main supervisors in different periods of my Ph.D. work and Dr. Jee-Hoon Jeong who served as assistant supervisor. Without their great guidance and invaluable supports based on their abundant knowledge, experience and the greatest patients, I could not have finished my Ph.D. work and the final thesis. A special thanks to Prof. Deliang Chen and his family, who have generously shared their knowledge and experiences both in research and life.

As a member of Regional Climate Group (RCG, http://rcg.gvc.gu.se/), I would like to thank all the past and present colleagues in the group, for the fruitful discussion and pleasant cooperation. Especially I wish to thank Dr. David Rayner, Dr. Christine Achberger, Dr. Elisabeth Simelton, Dr. Lin Tang and her husband Mr. Yongfeng Gu, Dr. Alexander Walther, Dr. Valerio Bartolino. Furthermore, I would also like to thank the present Ph.D. students in RCG, who are working with their research and thesis now, Staffan Rosell, Kristina Seftigen, Jesper Björklund, Peng Zhang, Andrea Seim, and Mauricio Fuentes. My best wishes to their research and thesis work.

Many thanks to Dr. Christian Stranne, Dr. Andreas Johnsson, Dr. Eskil Mattsson for their encouraging and Ms. Eugenia Andersson and Ms. Kerstin Ericson for the great help during my PhD study. Special thanks to the Nilsson family for their kindness and the happy time we had during the study period in Sweden and Dr. Zheng You and her husband Benjamin Fiedor for their great help in polishing English for this thesis.

Finally, this thesis is dedicated to my parents and my wife Yumei Hu as well as my sisters and their families.

References

Alexander, L. V., and Coauthors, 2006: Global observed changes in daily climate extremes of temperature and precipitation. *J Geophys Res-Atmos*, **111,** D05109.

Allan, R., and T. Ansell, 2006: A new globally complete monthly historical gridded mean sea level pressure dataset (HadSLP2): 1850-2004. *J Climate*, **19,** 5816-5842.

Bai, A., P. M. Zhai, and X. D. Liu, 2007: Climatology and trends of wet spells in China. *Theor Appl Climatol*, **88,** 139-148.

Barnes, R. J., 1991: The Variogram Sill and the Sample Variance. *Math Geol*, **23,** 673-678.

Chang, C. P., and K. M. W. Lau, 1980: Northeasterly Cold Surges and near-Equatorial Disturbances over the Winter Monex Area during December 1974 .2. Planetary-Scale Aspects. *Mon Weather Rev*, **108,** 298-312.

Chang, C. P., J. E. Erickson, and K. M. Lau, 1979: Northeasterly Cold Surges and near-Equatorial Disturbances over the Winter Monex Area during December 1974 .1. Synoptic Aspects. *Mon Weather Rev*, **107,** 812-829.

Chen, D., A. Walther, A. Moberg, P.D. Jones, J. Jacobeit, and D. Lister, 2006: Trend atlas of the EMULATE indices. ***Research Report*** C73, Earth Sciences Centre, Göteborg University, Gothenburg, Sweden, 797 pp.

Chen, C. T., and T. Knutson, 2008: On the verification and comparison of extreme rainfall indices from climate models. *J Climate*, **21,** 1605-1621.

Chang, C. P., K. M. Lau, and H. Hendon, 2006: The Asian winter monsoon, in *The Asian Monsoon*, edited by B. Wang, pp. 89-127, Springer Praxis, New York, doi:10.1007/3-540-37722-0_3.

Chen, D. L., T. H. Ou, L. B. Gong, C. Y. Xu, W. J. Li, C. H. Ho, and W. H. Qian, 2010: Spatial Interpolation of Daily Precipitation in China: 1951-2005. *Adv Atmos Sci*, **27,** 1221-1232.

Chen, T. C., W. R. Huang, and J. Yoon, 2004: Interannual variation of the east Asian cold surge activity. *J Climate*, **17,** 401-413.

Chen, Y., and Y. H. Ding, 2007: Cold air activities in July 2004 and its impact on intense rainfalls over Southwest China. *Acta Meteorol Sin*, **21,** 302-319.

DCAS/NCC/CMA (Division of Climate Application and Service, National Climate Center China Meteorological Administration), 2008: *Climate Events and Impacts in February of 2008*. Online: http://ncc.cma.gov.cn/influ/yxpj.php.

Ding, T., W.-H. Qian, and Z.-W. Yan, 2009: Characteristics and Changes of Cold Surge Events over China during 1960-2007. *Atmos. Oceanic Sci. Lett.*, **2,** 339−344.

Ding, Y., and T. N. Krishnamurti, 1987: Heat-Budget of the Siberian High and the Winter Monsoon. *Mon Weather Rev*, **115,** 2428-2449.

Ding, Y. H., 1990: Buildup, Air-Mass Transformation and Propagation of Siberian High and Its Relations to Cold Surge in East-Asia. *Meteorol Atmos Phys*, **44,** 281-292.

Ding, Y. H., and J. C. L. Chan, 2005: The East Asian summer monsoon: an overview. *Meteorol Atmos Phys*, **89,** 117-142.

Easterling, D. R., J. L. Evans, P. Y. Groisman, T. R. Karl, K. E. Kunkel, and P. Ambenje, 2000: Observed variability and trends in extreme climate events: A brief review. *B Am Meteorol Soc*, **81,** 417-425.

Feng, L., T. J. Zhou, B. Wu, T. Li, and J. J. Luo, 2011: Projection of Future Precipitation Change over China with a High-Resolution Global Atmospheric Model. *Adv Atmos Sci*, **28,** 464-476.

Feng, S., Q. Hu, and W. H. Qian, 2004: Quality control of daily meteorological data in China, 1951-2000: A new dataset. *Int J Climatol*, **24,** 853-870.

Franke, R., 1982: Scattered Data Interpolation - Tests of Some Methods. *Math Comput*, **38,** 181-200.

Frich, P., L. V. Alexander, P. Della-Marta, B. Gleason, M. Haylock, A. M. G. K. Tank, and T. Peterson, 2002: Observed coherent changes in climatic extremes during the second half of the twentieth century. *Climate Res*, **19,** 193-212.

Fu, J. L., W. H. Qian, X. Lin, and C. Deliang, 2008: Trends in graded precipitation in China from 1961 to 2000. *Adv Atmos Sci*, **25,** 267-278.

Gao, X. J., Z. C. Zhao, and F. Giorgi, 2002: Changes of extreme events in regional climate simulations over East Asia. *Adv Atmos Sci*, **19,** 927-942.

Garreaud, R. D., 2001: Subtropical cold surges: Regional aspects and global distribution. *Int J Climatol*, **21,** 1181-1197.

Gong, D. Y., and S. W. Wang, 2000: Severe summer rainfall in China associated with enhanced global warming. *Climate Res*, **16,** 51-59.

Gong, D. Y., and C. H. Ho, 2002: The Siberian High and climate change over middle to high latitude Asia. *Theor Appl Climatol*, **72,** 1-9.

——, 2004: Intra-seasonal variability of wintertime temperature over East Asia. *Int J Climatol*, **24,** 131-144.

Goovaerts, P., 2000: Geostatistical approaches for incorporating elevation into the spatial interpolation of rainfall. *J Hydrol*, **228,** 113-129.

Gu, W., and C.-y. Li, 2010: Evaluation of the IPCC AR4 Climate Models in Simulating the Interdecadal Variations of the East China Summer Precipitation, PDO and NAO. *Transactions of Atmospheric Sciences*, **33,** 11. (in Chinese with English abstract)

Hegerl, G. C., and Coauthors, 2006: Climate change detection and attribution: Beyond mean temperature signals. *J Climate*, **19,** 5058-5077.

Hong, C. C., H. H. Hsu, H. H. Chia, and C. Y. Wu, 2008: Decadal relationship between the North Atlantic Oscillation and cold surge frequency in Taiwan. *Geophys Res Lett*, **35,** L24707.

Hu, Z. Z., S. Yang, and R. G. Wu, 2003: Long-term climate variations in China and global warming signals. *J Geophys Res-Atmos*, **108**, 4614.

IPCC, 2007: *Climate Change 2007: The Physical Science Basis*. Contribution of Working Group I to the Fourth Assessment Report of the Intergovernmental Panel on Climate Change [Solomon, S., D. Qin, M. Manning, Z. Chen, M. Marquis, K.B. Averyt, M. Tignor, and H.L. Miller (eds.)]. Cambridge University Press, Cambridge, UK, 996 pp.

IPCC, 2012: *Managing the Risks of Extreme Events and Disasters to Advance Climate Change Adaptation.* A Special Report of Working Groups I and II of the Intergovernmental Panel on Climate Change [Field, C.B., V. Barros, T.F. Stocker, D. Qin, D.J. Dokken, K.L. Ebi, M.D. Mastrandrea, K.J. Mach, G.-K. Plattner, S.K. Allen, M.Tignor, and P.M. Midgley (eds.)]. Cambridge University Press, Cambridge, UK, and New York, NY, USA, 582 pp.

Jeong, J. H., and C. H. Ho, 2005: Changes in occurrence of cold surges over east Asia in association with Arctic Oscillation. *Geophys Res Lett*, **32,** L14704.

Jeong, J. H., C. H. Ho, B. M. Kim, and W. T. Kwon, 2005: Influence of the Madden-Julian Oscillation on wintertime surface air temperature and cold surges in east Asia. *J Geophys Res-Atmos*, **110,** D11104.

Jeong, J. H., T. H. Ou, H. W. Linderholm, B. M. Kim, S. J. Kim, J. S. Kug, and D. L. Chen, 2011: Recent recovery of the Siberian High intensity. *J Geophys Res-Atmos*, **116**, D23102.

Jiang, Z., J. Song, L. Li, W. Chen, Z. Wang, and J. Wang, 2011: Extreme climate events in China: IPCC-AR4 model evaluation and projection. *Climatic Change*, **110,** 385-401.

Kalnay, E., and Coauthors, 1996: The NCEP/NCAR 40-year reanalysis project. *B Am Meteorol Soc*, **77,** 437-471.

Kiktev, D., D. M. H. Sexton, L. Alexander, and C. K. Folland, 2003: Comparison of modeled and observed trends in indices of daily climate extremes. *J Climate*, **16,** 3560-3571.

Kunkel, K. E., R. A. Pielke, and S. A. Changnon, 1999: Temporal fluctuations in weather and climate extremes that cause economic and human health impacts: A review. *B Am Meteorol Soc*, **80,** 1077-1098.

Li, H. M., L. Feng, and T. J. Zhou, 2011: Multi-model Projection of July-August Climate Extreme Changes over China under CO(2) Doubling. Part I: Precipitation. *Adv Atmos Sci*, **28,** 433-447.

Lin, C. Y., S. C. C. Lung, H. R. Guo, P. C. Wu, and H. J. Su, 2009: Climate variability of cold surge and its impact on the air quality of Taiwan. *Climatic Change*, **94,** 457-471.

Linderholm, H. W., and Coauthors, 2011: Interannual teleconnections between the summer North Atlantic Oscillation and the East Asian summer monsoon. *J Geophys Res-Atmos*, **116**, D13107.

Liu, B. H., M. Xu, and M. Henderson, 2011: Where have all the showers gone? Regional declines in light precipitation events in China, 1960-2000. *Int J Climatol*, **31,** 1177-1191.

Liu, B. H., M. Xu, M. Henderson, Y. Qi, and Y. Q. Li, 2004: Taking China's temperature: Daily range, warming trends, and regional variations, 1955-2000. *J Climate*, **17,** 4453-4462.

Lu, Q. F., W. J. Zhang, P. Zhang, X. B. Wu, F. Y. Zhang, Z. Q. Liu, and M. B. Dale, 2010: Monitoring the 2008 cold surge and frozen disasters snowstorm in South China based on regional ATOVS data assimilation. *Sci China Earth Sci*, **53,** 1216-1228.

Ma, L. J., T. Zhang, O. W. Frauenfeld, B. S. Ye, D. Q. Yang, and D. H. Qin, 2009: Evaluation of precipitation from the ERA-40, NCEP-1, and NCEP-2 Reanalyses and CMAP-1, CMAP-2, and GPCP-2 with ground-based measurements in China. *J Geophys Res-Atmos*, **114**, D09105.

Meehl, G. A., and Coauthors, 2007: The WCRP CMIP3 multimodel dataset - A new era in climate change research. *B Am Meteorol Soc*, **88,** 1383-1394.

Meehl, G. A., and Coauthors, 2000: An introduction to trends in extreme weather and climate events: Observations, socioeconomic impacts, terrestrial ecological impacts, and model projections. *B Am Meteorol Soc*, **81,** 413-416.

Moberg, A., and Coauthors, 2006: Indices for daily temperature and precipitation extremes in Europe analyzed for the period 1901-2000. *J Geophys Res-Atmos*, **111**, D22106.

Munich-Reinsurance, 2002: Major natural catastrophes, 1950-2001. *Popul Dev Rev*, **28,** 171-174.

NCC (National Climate Center), 1998: China's 1998 Severe Flood and Climate Extremes, China's Meteorological Press, 137pp. (in Chinese)

New, M., M. Hulme, and P. Jones, 1999: Representing twentieth-century space-time climate variability. Part I: Development of a 1961-90 mean monthly terrestrial climatology. *J Climate*, **12,** 829-856.

Panagiotopoulos, F., M. Shahgedanova, A. Hannachi, and D. B. Stephenson, 2005: Observed trends and teleconnections of the Siberian high: A recently declining center of action. *J Climate*, **18,** 1411-1422.

Park, T. W., C. H. Ho, and S. Yang, 2011a: Relationship between the Arctic Oscillation and Cold Surges over East Asia. *J Climate*, **24,** 68-83.

Park, T. W., J. H. Jeong, C. H. Ho, and S. J. Kim, 2008: Characteristics of Atmospheric Circulation Associated with Cold Surge Occurrences in East Asia: A Case Study During 2005/06 Winter. *Adv Atmos Sci*, **25,** 791-804.

Park, T. W., C. H. Ho, S. J. Jeong, Y. S. Choi, S. K. Park, and C. K. Song, 2011b: Different characteristics of cold day and cold surge frequency over East Asia in a global warming situation. *J Geophys Res-Atmos*, **116**, D12118.

Qian, W. H., and D. K. Lee, 2000: Seasonal march of Asian summer monsoon. *Int J Climatol*, **20,** 1371-1386.

Qian, W. H., J. K. Fu, and Z. W. Yan, 2007a: Decrease of light rain events in summer associated with a warming environment in China during 1961-2005. *Geophys Res Lett*, **34**, L11705.

Qian, W. H., D. Chen, Y. Zhu, and H. Y. Shen, 2003: Temporal and spatial variability of dryness/wetness in China during the last 530 years. *Theor Appl Climatol*, **76,** 13-29.

Qian, W. H., X. Lin, Y. F. Zhu, Y. Xu, and J. L. Fu, 2007b: Climatic regime shift and decadal anomalous events in China. *Climatic Change*, **84,** 167-189.

Qian, Y., D. Y. Gong, J. W. Fan, L. R. Leung, R. Bennartz, D. L. Chen, and W. G. Wang, 2009: Heavy pollution suppresses light rain in China: Observations and modeling. *J Geophys Res-Atmos*, **114,** D00K02.

Ren, G., and Coauthors, 2011: Change in climatic extremes over mainland China based on an integrated extreme climate index. *Climate Res*, **50,** 113-124.

Rummukainen, M., 2012: Changes in climate and weather extremes in the 21st century. *Wires Clim Change*, **3,** 115-129.

Su, B. D., B. Xiao, D. M. Zhu, and T. Jiang, 2005: Trends in frequency of precipitation extremes in the Yangtze River basin, China: 1960-2003. *Hydrolog Sci J*, **50,** 479-492.

Taylor, K. E., R. J. Stouffer, and G. A. Meehl, 2012: An Overview of CMIP5 and the Experiment Design. *B Am Meteorol Soc*, **93,** 485-498.

Trenberth, K. E., and D. A. Paolino, 1980: The Northern Hemisphere Sea-Level Pressure Data Set - Trends, Errors and Discontinuities. *Mon Weather Rev*, **108,** 855-872.

Uppala, S. M., and Coauthors, 2005: The ERA-40 re-analysis. *Q J Roy Meteor Soc*, **131,** 2961-3012.

Walther, A., J. H. Jeong, G. Nikulin, C. Jones, and D. L. Chen, 2013: Evaluation of the warm season diurnal cycle of precipitation over Sweden simulated by the Rossby Centre regional climate model RCA3. *Atmos Res*, **119,** 131-139.

Wang, H. J., 2001: The weakening of the Asian monsoon circulation after the end of 1970's. *Adv Atmos Sci*, **18,** 376-386.

Wang, H. J., and Coauthors, 2012: Extreme Climate in China: Facts, Simulation and Projection. *Meteorol Z*, **21,** 279-304.

Wang, L., and W. Chen, 2010: How well do existing indices measure the strength of the East Asian winter monsoon? *Adv Atmos Sci*, **27,** 855-870.

Wang, L., R. H. Huang, L. Gu, W. Chen, and L. H. Kang, 2009: Interdecadal Variations of the East Asian Winter Monsoon and Their Association with Quasi-Stationary Planetary Wave Activity. *J Climate*, **22,** 4860-4872.

Wang, Y., and Z. W. Yan, 2009: Trends in Seasonal Precipitation over China during 1961−2007. *Atmospheric and Oceanic Science Letter*, **2,** 165−171.

Wang Z. Y., and Y.H. Ding, 2006: Climate change of the cold wave frequency of China in the last 53 years and the possible reasons. *Chinese Journal of Atmospheric Sciences*, **30**, 1068-1076. (in Chinese with English abstract)

Wu, B. Y., and J. Wang, 2002: Winter Arctic Oscillation, Siberian High and East Asian winter monsoon. *Geophys Res Lett*, **29,** 1897.

Wu, M. C., and J. C. L. Chan, 1995: Surface-Features of Winter Monsoon Surges over South China. *Mon Weather Rev*, **123,** 662-680.

——, 1997: Upper-level features associated with winter monsoon surges over south China. *Mon Weather Rev*, **125,** 317-340.

Wu, R. G., J. L. Kinter, and B. P. Kirtman, 2005: Discrepancy of interdecadal changes in the Asian region among the NCEP-NCAR reanalysis, objective analyses, and observations. *J Climate*, **18,** 3048-3067.

Xu, C. H., Y. Luo, and Y. Xu, 2011: Projected changes of precipitation extremes in river basins over China. *Quatern Int*, **244,** 149-158.

Xu, Y., X. J. Gao, Y. Shen, C. H. Xu, Y. Shi, and F. Giorgi, 2009: A Daily Temperature Dataset over China and Its Application in Validating a RCM Simulation. *Adv Atmos Sci*, **26,** 763-772.

Yang, G. M., Q. Kong, D. Y. Mao, F. H. Zhang, Z. M. Kang, and Z. P. Zong, 2010: Analysis on the Long-Lasting Freezing Rain and Snowstorm Event at the Beginning of 2008. *Acta Meteorol Sin*, **24,** 380-396.

Yang, J., and D. Y. Gong, 2010: Intensified reduction in summertime light rainfall over mountains compared with plains in Eastern China. *Climatic Change*, **100,** 807-815.

Yang, T. C., P. C. Wu, V. Y. J. Chen, and H. J. Su, 2009: Cold surge: A sudden and spatially varying threat to health? *Science of the Total Environment*, **407,** 3421-3424.

You, Q. L., and Coauthors, 2011: Changes in daily climate extremes in China and their connection to the large scale atmospheric circulation during 1961-2003. *Clim Dynam*, **36,** 2399-2417.

Yu, R. C., and T. J. Zhou, 2007: Seasonality and three-dimensional structure of interdecadal change in the East Asian monsoon. *J Climate*, **20,** 5344-5355.

Yu, R. C., B. Wang, and T. J. Zhou, 2004: Tropospheric cooling and summer monsoon weakening trend over East Asia. *Geophys Res Lett*, **31,** L22212.

Zhai, P. M., X. B. Zhang, H. Wan, and X. H. Pan, 2005: Trends in total precipitation and frequency of daily precipitation extremes over China. *J Climate*, **18,** 1096-1108.

Zhai, P.M., Z.W. Yan and X.K. Zhou, 2008: Climate Extremes and Related Disasters in China. In: *Regional Climate Studies of China* [Fu, C.B., Z.H. Jiang, Z.Y. Guan., J.H. He and Z.F. Xu (eds.)]. Springer Berlin, Heidelberg, pp. 313-344.

Zhang, P. Z., and G. M. Chen, 1999: A statistical analysis of the cold wave high which influences on China. *Acta Meteorol Sin*, **57,** 493-501. (in Chinese with English abstract)

Zhang, Y., K. R. Sperber, and J. S. Boyle, 1997: Climatology and interannual variation of the East Asian winter monsoon: Results from the 1979-95 NCEP/NCAR reanalysis. *Mon Weather Rev*, **125,** 2605-2619.

Zhao, L.N., Q.Y. Ma, G.M. Yang, X.R. Wang, L.Q. Zhao, X.D. Yang, H. Wu, Z. Wang, Z.M. Kang**,** and D.Y. Mao, 2008: Disasters and its impact of a sever snow storm and freezing rain over southern China in January 2008. *Climatic and Environmental Research*, **13**, 556-566. (in Chinese with English abstract)

Zhou, T. J., and Coauthors, 2009: The CLIVAR C20C project: which components of the Asian-Australian monsoon circulation variations are forced and reproducible? *Clim Dynam*, **33,** 1051-1068.

Zhu, Y. F., 2008: An Index of East Asian Winter Monsoon Applied to the Description of China's Mainland Winter Temperature Changes. *Acta Meteorol Sin*, **22,** 522-529.